TREE CROWN DETECTION USING MULTISPECTRAL SATELLITE IMAGERY

A THESIS SUBMITTED TO
THE GRADUATE SCHOOL OF INFORMATICS OF
THE MIDDLE EAST TECHNICAL UNIVERSITY
BY

MEHMET MERT ONAĞ

IN PARTIAL FULFILLMENT OF THE REQUIREMENTS FOR THE DEGREE
OF
MASTER OF SCIENCE
IN
THE DEPARTMENT OF INFORMATION SYSTEMS

MAY 2018

Approval of the thesis:

TREE CROWN DETECTION USING MULTISPECTRAL SATELLITE IMAGERY

Submitted by MEHMET MERT ONAĞ in partial fulfillment of the requirements for the degree of **Master of Science in Information Systems Department, Middle East Technical University** by,

Prof. Dr. Deniz Zeyrek Bozşahin _____
Dean, **Informatics Institute**

Prof. Dr. Yasemin Yardımcı Çetin _____
Head of Department, **Information Systems**

Prof. Dr. Yasemin Yardımcı Çetin _____
Supervisor, **Information Systems Dept., METU**

Examining Committee Members:

Assoc. Prof. Dr. Banu Günel Kılıç _____
Information Systems Dept., METU

Prof. Dr. Yasemin Yardımcı Çetin _____
Information Systems Dept., METU

Assoc. Prof. Dr. Uğur Murat Leloğlu _____
Geodetic and Geographic Information Tech. Dept., METU

Assoc. Prof. Dr. Alptekin Temizel _____
Multimedia Informatics Dept., METU

Assist. Prof. Dr. Seniha Esen Yüksel _____
Electrical and Electronics Eng. Dept., Hacettepe University

Date: 16 May 2018

I hereby declare that all information in this document has been obtained and presented in accordance with academic rules and ethical conduct. I also declare that, as required by these rules and conduct, I have fully cited and referenced all material and results that are not original to this work.

Name, Last name : Mehmet Mert ONAĞ

Signature : _____

ABSTRACT

TREE CROWN DETECTION USING MULTISPECTRAL SATELLITE IMAGERY

ONAĞ, Mehmet Mert

MSc., Department of Information Systems

Supervisor: Prof. Dr. Yasemin Yardımcı Çetin

May 2018, 76 pages

Forests have an essential place in our lives because they provide various components for source of life. In parallel with the growing environmental awareness, the importance of forests has increased in recent years. Forestry policy of a country predominantly depends on its regional forest inventory. However, the establishment of forest inventories in areas with large forest areas is a demanding time-consuming and expensive process due to physical constraints.

This thesis aims to detect trees in very high resolution multispectral satellite images, in particular WorldView-2 and WorldView-3 which provide eight spectral bands in the visible near infrared (VNIR) region. The first step of tree detection process is detecting vegetated areas from satellite imagery. For this purpose, different vegetation indices used by other researchers as well as some novel vegetation indices and their combinations are analyzed. In this step, different thresholds are experimented for vegetation indices to improve accuracy. Tree crowns in vegetated areas are determined by local maxima of NIR1 band of the satellite images. In this step, local maxima algorithm is utilized for detecting treetops. Low pass filtering is applied before local maxima detection to improve accuracy. After finding local peaks, shadowy areas are detected and their positions are validated by the trees detected earlier to eliminate false detections such as grass. The proposed method achieved better overall performance when compared with similar tree detection methods.

Keywords: multispectral satellite imagery, WorldView, NDVI, tree crown detection, shadow detection

ÖZ

MULTISPEKTRAL UYDU İMGELERİNDEN AĞAÇ TAÇLARININ TESPİT EDİLMESİ

ONAĞ, Mehmet Mert

Yüksek Lisans, Bilişim Sistemleri Bölümü

Tez Yöneticisi: Prof. Dr. Yasemin Yardımcı Çetin

Mayıs 2018, 76 sayfa

Ormanlar hayatımızda önemli bir yere sahiptir, çünkü ormanlar yaşamın kaynağı olan çeşitli bileşenleri sağlar. Son yıllarda artan çevre bilincine paralel olarak, ormanların önemi daha da artmaya başlamıştır. Bir ülkenin ormancılık politikası, ağırlıklı olarak bölgesel orman envanterine bağlıdır. Ancak, geniş ormanlık alanlarda orman envanterlerinin tespit edilmesi, fiziksel kısıtlamalar nedeniyle zaman alıcı ve pahalı bir süreçtir.

Bu tez, görünür yakın kızılötesinde sekiz spektral bant sağlayan WorldView-2 ve WorldView-3 çok yüksek çözünürlüklü multispektral uydu imgelerinden ağaçların tespit edilmesini hedefler. Ağaç tespit sürecinin ilk adımı, uydu görüntülerinden bitki örtüsü içeren alanları tespit etmektir. Bu amaçla, diğer araştırmacılar tarafından kullanılan farklı bitki örtüsü indeksleri ve bazı yeni bitki örtüsü indeksleri ve bunların birleşimleri analiz edilmiştir. Bu adımda, doğruluk oranını artırmak için farklı eşik değerleri denemiştir. Bitkisel alanlardaki ağaç taçları, uydu görüntülerinin yakın kızılötesi bandının yerel maksimumu ile belirlenmiştir. Bu adımda, ağaç tepelerinin tespiti için yerel maksimum algoritması kullanılmıştır. Doğruluğu iyileştirmek için yerel maksimum bulma işleminden önce düşük frekans geçişli filtreleme uygulanmıştır. Yerel maksimumları bulduktan sonra, çim gibi yanlış tespitleri ortadan kaldırmak için gölgeli alanlar ve tespit edilen noktalara göre bu alanların yerleri tespit edilmiştir. Önerilen yöntemin genel performansı, benzer ağaç algılama yöntemleri ile karşılaştırıldığında daha doğru sonuçlar verdiği görülmüştür.

Anahtar Sözcükler: multispektral uydu imgesi, WorldView, normalize edilmiş fark bitki örtüsü indeksi, ağaç tacı tespit etme, gölge tespit etme

DEDICATION

To My Family

ACKNOWLEDGEMENTS

First of all, I would like to express my thankfulness and also appreciation to my supervisor Prof.Dr. Yasemin Yardımcı Çetin for her fortitude, invaluable guidance, endless support and helpful approach throughout my research.

Besides my supervisor, I would like to thank Okan Bilge Özdemir for his encouragement, technical troubleshooting and guidance. He has helped whenever I need a hand both technically and mentally.

I would also like to thank Assoc. Prof. Dr. Banu Günel Kılıç, Assoc. Prof. Dr. Uğur Murat Leloğlu, Assoc. Prof. Dr. Alptekin Temizel and Asst. Prof. Dr. Seniha Esen Yüksel for reviewing my work.

Finally, I would like to thank my family because of their never ending support. They made me feel that they were constantly side with me from hundreds of kilometers.

TABLE OF CONTENTS

LIST OF TABLES

LIST OF FIGURES

CHAPTER 1

INTRODUCTION

1.1 Motivation

Research in the area of remote sensing is one of the most popular topics of the recent years. With the development of very high resolution multispectral satellite sensors, more information about earth surface like sea, soil, vegetation, or manmade objects is extracted from satellite images in a cost effective way.

While green vegetation absorb solar radiation in the visible red band to do photosynthesis, they reflect solar radiation in near infrared spectral region to avoid over-heating and harm themselves [1]. Since many multispectral satellite sensors provide information on infrared spectral bands as well as on visible bands, detecting individual tree crowns from satellite imagery using this contrast has begun to be one of the valuable research areas in satellite image processing. Moreover, detection of tree crowns can help to keep inventory of trees and to analyze number of them through the time in both urban and rural areas.

Tree crown detection process starts with detecting vegetated areas from satellite imagery. To investigate this phenomenon, vegetation indices are developed for determining the pixels belonging to vegetation areas. Since tree crowns and other vegetated areas like grass or shrub show similar spectral characteristics, discriminating tree crowns and other vegetated areas is a challenging problem. Therefore, without discriminating tree crown and other vegetated areas, acquiring accurate results may not be possible. Thus, the main objective of treetop detection is identifying the trees in satellite imagery when other vegetated areas are present. On the other hand, the requirement of tree crown detection from identified vegetated areas is also a complicated process. Because, when the frequency and variations in the size of tree crowns increases, identification of treetops becomes more demanding.

1.2 Scope and goal

This study is dedicated to detecting tree crowns from remotely sensed data. WorldView-2 and WorldView-3 multispectral images that provide 8 different spectral bands with high spectral resolution are used. Seven different scenes (four WorldView-2 and three WorldView-3) are cropped from these images for experiments. The main objectives of this study are listed below:

- To identify of tree crowns from vegetated areas that extracted by the vegetation indices.
- To determine the vegetation index that gives best results among other vegetation indices.
- To propose some novel vegetation indices to detect vegetated areas accurately.
- To analyze local maxima detection algorithm for detecting treetops by using different window sizes and low pass filters.
- To analyze the contribution of treetop validation by shadowy areas according to their positions to discriminate treetops and grass.

1.3 Outline of thesis

This thesis is organized as five chapters including introduction, background, methodology, experiments and conclusion. In Chapter 2, literature survey on pan-sharpening, vegetation indices, tree crown detection, and shadow detection is provided. Moreover, the data that is used in this study, the proposed tree crown detection method, pre-processing method, and vegetation indices are described in Chapter 3. Also, novel vegetation indices are proposed in this chapter. Chapter 4 presents experiments, accuracy results and their comparison for the proposed methods. Finally, the thesis is finalized with a summary of our research and possible future work for this study is stated in Chapter 5.

CHAPTER 2

BACKGROUND

Remote sensing is the term that refers to gathering information about physical objects from a distance without physical contact. This valuable information about earth surface can be acquired by sensors stationed on ground vehicles, aircraft (airborne) or satellites (spaceborne) [2]. These sensors can be classified into two primary categories as active and passive sensors. The active types of sensors transmit pulses of energy and receive the reflected pulses of energy from the Earth's surface. On the other hand, the passive type of sensors measure emitted energy from the atmosphere, surface or transmitted from the subsurface [3]. Depiction of passive and active remote sensing can be seen in Figure 1. Since different objects can show different spectral reflectance by reflecting or absorbing different wavelengths, these objects can be classified according to their spectral reflectance [2].

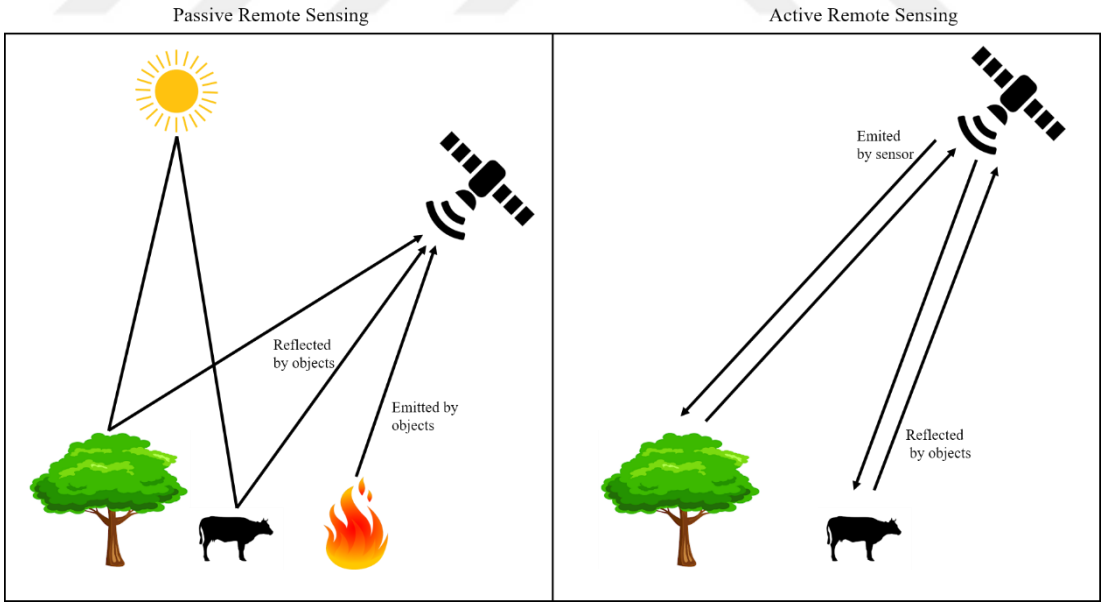

Figure 1: Passive and active remote sensing

Most of the active sensors make use of microwave part of the electromagnetic spectrum, whereas the majority of the passive sensors operate in the visible, infrared, thermal infrared, as well as the microwave part of the electromagnetic spectrum [4]. Figure 2 shows the electromagnetic spectrum.

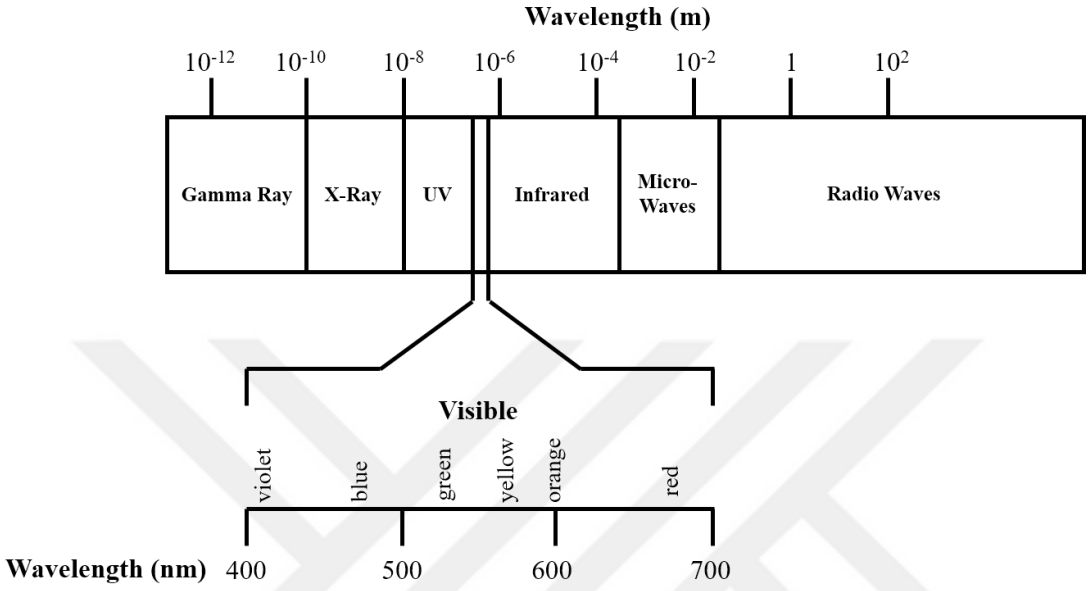

Figure 2: Electromagnetic spectrum

Optical and infrared passive remote sensors can be classified into three different categories according to the spectral bands used in the sensing process. These systems are called panchromatic imaging systems, multispectral imaging systems, and hyperspectral imaging systems.

Panchromatic imaging systems utilize a single channel sensor. This sensor is sensitive to radiation within a wide wavelength range. These systems measure the apparent brightness of the objects disregarding the spectral information. Consequently, the result of imaging system shows a "black-and-white" image. WorldView-1, IKONOS PAN, and QuickBird PAN are examples of this type of imaging systems.

Multispectral imaging systems use multichannel sensors with three or more spectral bands. These channels usually sense the radiation within a narrow bandwidth. The output images contain both spectral and brightness information. IKONOS MS, LANDSAT MS, WorldView-2 MS are examples for multispectral imaging systems.

Hyperspectral imaging systems, which are also known as “imaging spectrometers”, have typically 100 or more spectral contiguous bands. These imaging systems provide precise spectral information about target objects. Hyperion, ROSIS and AVIRIS are some examples of hyperspectral imaging systems [5].

In recent decades, multispectral very high spatial resolution satellites were launched, hence detailed information of the objects on earth's surface can be easily accessed [6]. Vegetated areas are effectively extracted using VNIR (visible and near infrared) and/or SWIR (short-wave infrared) bands. Multispectral satellites can often gather information about these bands. Figure 3 shows spectral response patterns -also called spectral signatures- of grass, soil and water.

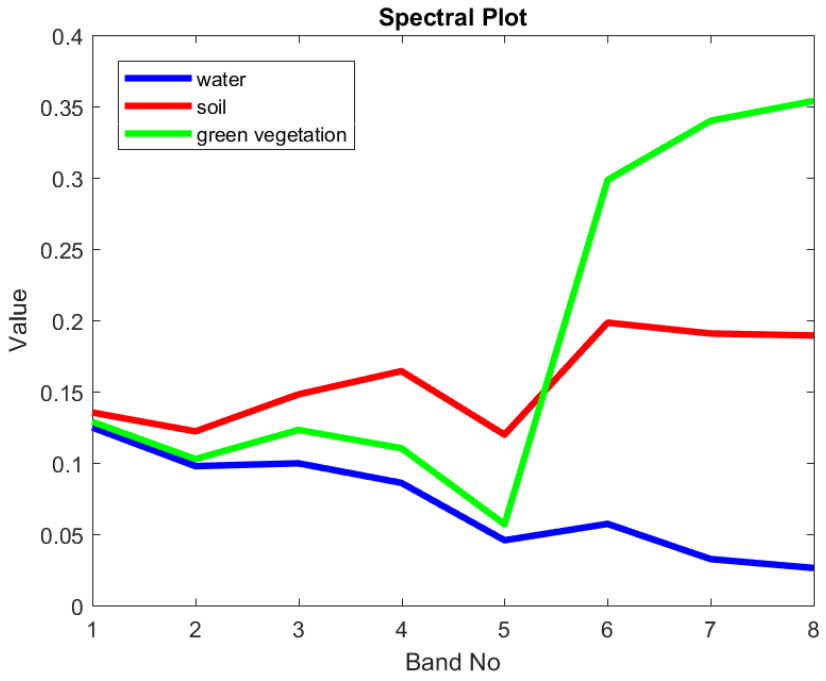

Figure 3: Spectral response patterns

There are some issues in multispectral image processing. Firstly, spectral signature of the same object can be different in different images due to positioning and properties of the sensor, meteorological conditions, or image acquisition date and time. Also, there is a trade-off between spatial and spectral resolution. The square of ground imaged by a single pixel corresponds to the spatial resolution of a sensor, whereas the spectral resolution can be defined as the granularity of the electromagnetic spectrum that a sensor will detect. Although one pixel of a multispectral image can store more spectral information than panchromatic images, it has lower spatial resolution as illustrated in Figure 4.

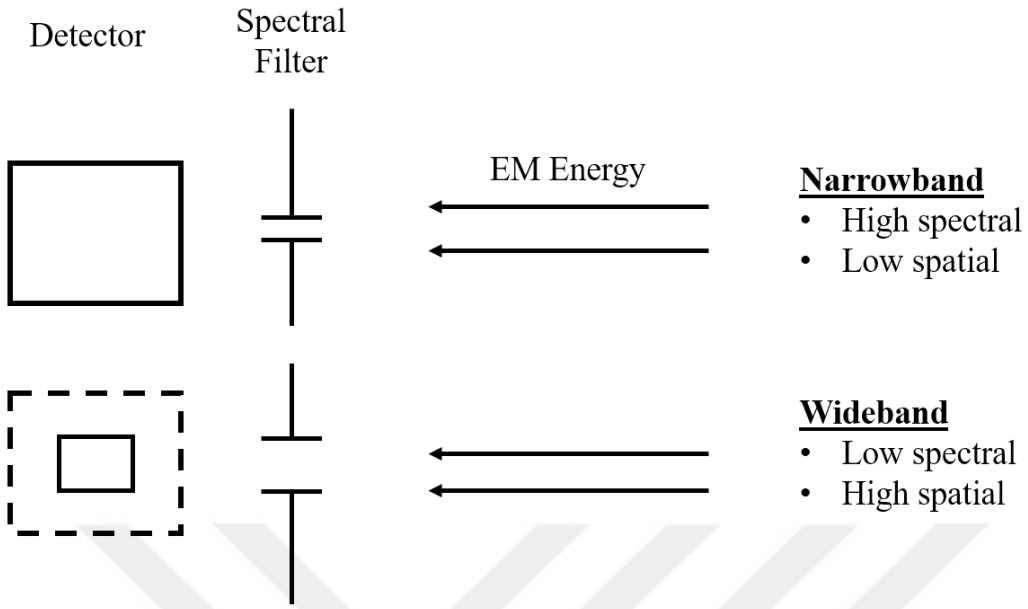

Figure 4: Spectral vs. spatial resolution

These challenges can be overcome by various multispectral image processing methods. For instance, pan-sharpening methods can be used to incorporate higher spatial resolution of the panchromatic images into corresponding multispectral image. These techniques fuse the low spatial resolution multispectral image and high spectral resolution multispectral image and produce higher spatial resolution multispectral image.

2.1 Literature Survey

In this thesis, multispectral imagery is pre-processed using a pan-sharpening algorithm for higher spatial resolution. Hyperspherical Color Sharpening (HCS) method is utilized for this purpose. For vegetation detection from multispectral satellite imagery, various vegetation indices are experimented for masking non-vegetated areas. Furthermore, local maxima detection method is utilized as tree crown finder from masked satellite imagery. Finally, shadows are detected to eliminate the trees which are presupposed as tree crowns.

2.1.1 HCS Pan-Sharpening

In high resolution multispectral imagery, panchromatic image has usually higher resolution than multispectral image. Therefore, most of the researchers utilized various pan-sharpening algorithms for obtaining high resolution multispectral images. I preferred to take advantage of HCS algorithm designed by Padwick et al. in this study.

They reported that the HCS algorithm can handle any number of input spectral bands and so the method is suitable for WorldView-2 imagery. This algorithm gets all of the bands of imagery as input and produces same number of sharpened spectral bands. They proposed two modes of algorithm: naïve and smart mode[7].

Immitzer et al. utilized the HCS algorithm for sharpening WorldView-2 image to classify tree species using Random Forest classifier [8]. Another study that utilized HCS algorithm is performed by Karlson et al. They implemented the HCS algorithm on WorldView-2 image as preprocessing step of tree crown mapping process [9].

Detailed information about this algorithm is described in Section 3.2.

2.1.2 Vegetation Indices

Vegetation index is a spectral transformation of two or more bands to detect vegetated areas or to determine vegetation properties [10]. Since number of spectral bands provided by multispectral sensors increased through decades, different vegetation indices utilizing different spectral bands derived. In this study, I examined thirteen different vegetation indices utilized by other researchers for extracting tree crowns on multispectral imagery. These will be introduced in this section. I found out Normalized Difference Vegetation Index (NDVI) utilizing NIR1 band of WorldView-2 and WorldView-3 imagery produced better results than others.

2.1.2.1 Excess Green

Excess green index (ExG) is visible spectral band based vegetation index designed by Woebbecke et al. (1995) to identity greenness of vegetation [11]. Calculation of Excess Green starts with applying normalization of spectral components.

$$g = \frac{G}{R+G+B}, r = \frac{R}{R+G+B}, b = \frac{B}{R+G+B} \quad (1)$$

These normalized values (g, r, b) are in the range [0, 1]. Then, Excess Green index is computed according to following equation:

$$ExG = 2g - r - b \quad (2)$$

Guijarro et al. used ExG index for segmentation of textures in agricultural images that include green plants, soil and the sky. The authors combined ExG index with other indices for detecting green plants. The index gave acceptable results for greenness detection [12]. Srestasathiern and Rakwatin used the index as candidate feature for detecting oil palm trees. However, ExG index produced very poor results for detecting oil palm trees [13]. Yang et al. utilized ExG index to identify greenness of crop images. Usage of the index in general produced good performance [14].

2.1.2.2 Excess Red

Excess red index (ExR) is visible spectral band based vegetation index that is proposed by Meyer and Neto (1998) for vegetation separation [15]. Calculation of ExR index starts with applying normalization of spectral components.

$$g = \frac{G}{R+G+B}, r = \frac{R}{R+G+B}, b = \frac{B}{R+G+B} \quad (3)$$

These normalized values (g, r, b) are in the range [0, 1]. Then, ExR index is computed according to following equation.

$$ExR = 1.4r - g \quad (4)$$

Guijarro et al. also used the ExR index. The authors utilized the index especially for soil detection [12]. On the other hand, Srestasathiern and Rakwatin considered ExR index for discriminating oil palm trees from background. The total dissimilarity metric of ExR index showed that ExR index was relatively good for discriminating oil palm trees and background but better results were obtained from other vegetation indices [13].

2.1.2.3 Excess Blue

Excess blue index (ExB) is visible spectral band based vegetation index that is proposed by Guijarro et al. (2011) as a simple translation of ExR index. They used the ExB index to identify blueness for detecting sky parts of agricultural images [12]. The ExB index is calculated by changing red component of ExR index by the blue one.

$$ExB = 1.4b - g \quad (5)$$

Another index which was analyzed by Srestasathiern and Rakwatin is excess blue. The index produced average result for discriminating oil palm trees and background [13].

2.1.2.4 Excess Green - Excess Red

Excess Green - Excess Red index (ExGR) is derived by subtracting ExR index from ExG index and introduced by Neto (2004) [16]. Formulation of the index is shown below:

$$ExGR = ExG - ExR = 2g - 2.4r - b \quad (6)$$

They used the index to separate pigweed and velvetleaf from soil background. Meyer and Neto utilized the index for automated crop imaging applications. The ExGR index showed better results for vegetation separation when compared to other vegetation indices that are analyzed in the study [15]. Srestasathiern and Rakwatin used the index as candidate index for oil palm tree detection. But, their analysis showed that the ExGR index gave poor results for oil palm tree detection [13]. Guijarro et al. also utilized this index to identify three components of scenes including green plants, soil and sky in agricultural images. They obtained satisfying results by using the index for greenness detection for segmenting and classifying vegetated areas [12].

2.1.2.5 Normalized Difference Index

Normalized Difference Index (NDI) is firstly proposed by Tucker (1979) as "Green – Red Vegetation Index" for assessing the relationships between the vegetation index and biomass, leaf water and chlorophyll content. [17]. Perez et al. utilized this vegetation index for weed detection in cereal fields [18]. NDI is calculated by using green and red bands and is given as:

$$NDI = \frac{G - R}{G + R} \quad (7)$$

Falkowski et al. utilized the index for characterizing and mapping forest fire fuels [19]. Motohka et al. used the index as vegetation phenological indicator. Their study showed that NDVI is not sensitive enough to seasonal color changes of leaves. They utilized NDI to monitor leaf coloring [20]. NDI is also among the vegetation indeces utilized by Waser et al. It is used in a classification algorithm (multinomial logistic regression technique) as an explanatory variable [21]. Srestasathiern and Rakwatin used the index as candidate index for oil palm tree detection and this index had the highest dissimilarity metric in the study [13]. Meyer and Neto utilized the index with Otsu threshold for automated crop imaging applications. Although the index showed poor results for vegetation detection, it worked well for the bare soils [15].

2.1.2.6 Green Normalized Difference Vegetation Index

Green Normalized Difference Vegetation Index (GNDVI) is proposed by Gitelson et al. (1996) by replacing the red component of NDVI with the green component [22]. GNDVI is calculated by using NIR and green bands and is given as:

$$GNDVI = \frac{NIR - G}{NIR + G} \tag{8}$$

Srestasathiern and Rakwatin utilized the index for oil palm tree detection. The result of discrimination analysis of the index showed that GNDVI produced poor dissimilarity metrics [13]. Waser et al. used the index as another explanatory variable of classification algorithm that classifies seven different tree species and different levels of damaged ash [21]. Hunt et al. utilized the index to measure crop biomass remotely. They proposed to use the index instead of NDVI in NIR-green-blue in digital images that lack the red bands [23].

2.1.2.7 NIR2-Yellow Vegetation Index

NIR2-Yellow Vegetation Index (NYVI) is used by Waser et al. (2014) to classify tree species and levels of ash mortality. The index is employed in explanatory variables of multinomial logistic regression [21]. The calculation of the index is based on normalized difference of NIR2 and yellow components of multispectral imagery and calculated as given below:

$$NYVI = \frac{NIR2 - Y}{NIR2 + Y} \tag{9}$$

Nouri et al. investigated five combinations of eight spectral bands of WorldView-2 images for finding relationship between vegetation indices and temporal urban landscape evapotranspiration factors and one of the combinations was NYVI. However, results of their analysis showed that NDVI is the most reliable vegetation index among the five vegetation indices [24].

2.1.2.8 RedEdge-Yellow Vegetation Index

RedEdge-Yellow Vegetation Index (REY) was firstly proposed by Gwata in 2012 for terrain classification purposes. Gwata analyzed also new spectral bands of WorldView-2 for vegetation detection [25]. Calculation of REY is similar with NDVI except that RedEdge and Yellow bands are used as components of the vegetation index for the calculation.

$$REY = \frac{RE - Y}{RE + Y} \quad (10)$$

Waser et al. also used the index as one of the variable of multinomial logistic regression techniques [21].

2.1.2.9 NIR1-Red-yellow Ratio Vegetation Index

Gwata defined and utilized the NIR1-Red-yellow Ratio Vegetation Index (NIRRY) as input for classification algorithm in 2012. Gwata's study showed that the index was successful for differentiating healthy and unhealthy vegetation [25]. The index is calculated as given below:

$$NIRRY = \frac{NIR1}{R + Y} \quad (11)$$

Waser et al. utilized the index for classifying trees and detecting different levels of tree damage [21].

2.1.2.10 Normalized Red Index

Within the recent decades, Normalized Red Index (NR) was firstly proposed by Sripada for defining in-season nitrogen needs for corn [26]. NR is calculated by normalizing red band and is given as:

$$NR = \frac{R}{NIR1 + R + G} \quad (12)$$

Srestasathiern and Rakwatin utilized NR as a candidate index for oil palm tree detection. However, the index did not provide sufficient distinctive results for oil palm tree detection [13]. NR is also used by Verma et al. for classification of LISS IV imagery. The index took place in proposed decision tree as a node and finally they produced eight classes (water, fallow, settlement, poplar tree, orchard, sugarcane, paddy, sorghum) [27].

2.1.2.11 Normalized NIR1 Index

Another vegetation index which was proposed by Sripada (2005) is Normalized NIR index (NNIR). The index is used for the same purposes as NR [26]. NNIR is calculated by normalizing NIR1 band as given below:

$$NNIR = \frac{NIR1}{NIR1 + R + G} \tag{13}$$

NNIR is also used by Srestasathiern and Rakwatin for oil palm tree detection. However, NNIR gave poor results according to calculated dissimilarity metrics [13]. Another study that used the index is made by Verma et al. to classify LISS IV imagery. One node of proposed decision tree included NNIR value for classification [27].

2.1.2.12 Normalized Difference Vegetation Index

Normalized difference vegetation index (NDVI) was firstly developed in 1973 by Rouse et al. for monitoring vegetation conditions in the Great Plains [28]. The index defined as the difference of NIR band and red band divided by their sum as shown below:

$$NDVI = \frac{NIR - R}{NIR + R} \tag{14}$$

NDVI has been the choice of many researchers for vegetation detection over the years [29]. Nouri et al. utilized NDVI for investigating relationship between different combinations of normalized difference vegetation indices and temporal urban landscape evapotranspiration factors. Their study showed that NDVI with NIR1 of WorldView-2, hence NDVI1, gave best results among the five combinations of normalized difference vegetation indices [24]. Gwata used the index for vegetation detection and as input for classification algorithm to extract various vegetation classes using different bands of WorldView-2 imagery [25]. Verma et al. also utilized the index in decision tree classification to classify water, fallow, settlement and five different species of vegetation. They employed Indian satellite IRS-P6, LISS-IV sensor's forth band as NIR band [27].

As WorldView-2 satellite has two different NIR bands, some researchers have investigated the potential of each NIR band. Eckert referred normalized difference vegetation index-2 (NDVI2)

$$NDVI2 = \frac{NIR2 - R}{NIR2 + R} \tag{15}$$

to develop biomass and carbon estimation models for humid rainforest. However, NDVI2 did not show good correlation between biomass and carbon [30].

Marshall et al. tried to detect buffel grass and for that purpose utilized the index for extracting vegetation components of land cover from the WorldView-2 multispectral satellite image [31]. However, Santos and Freire reported that NDVI2 did not capture photosynthetic activity as well as the NDVI1 [32]. The same issue is also addressed by Nouri et al [24].

2.1.3 Local Maxima Detection

In order to find treetops from the multispectral satellite imagery, local maxima detection algorithm is used by various researchers. The main idea of detecting treetops by using local maxima detection algorithm is based on two principal assumptions. The first assumption is that the spectral reflectance of the treetop is higher than the other parts of tree crown. As for the second assumption, the spectral reflection decreases along the downward direction from the treetop [33]. Wulder et al. performed study for investigating the use of local maximum filtering for detecting tree locations from high spatial resolution imagery. They correctly detected 67% of the trees within the focused area [34]. As is seen in Figure 5, treetops show higher spectral reflectance. Since tree crowns on multispectral satellite images are often not unimodal a Gaussian low pass filter is applied on the multispectral satellite image before local maxima detection process [35].

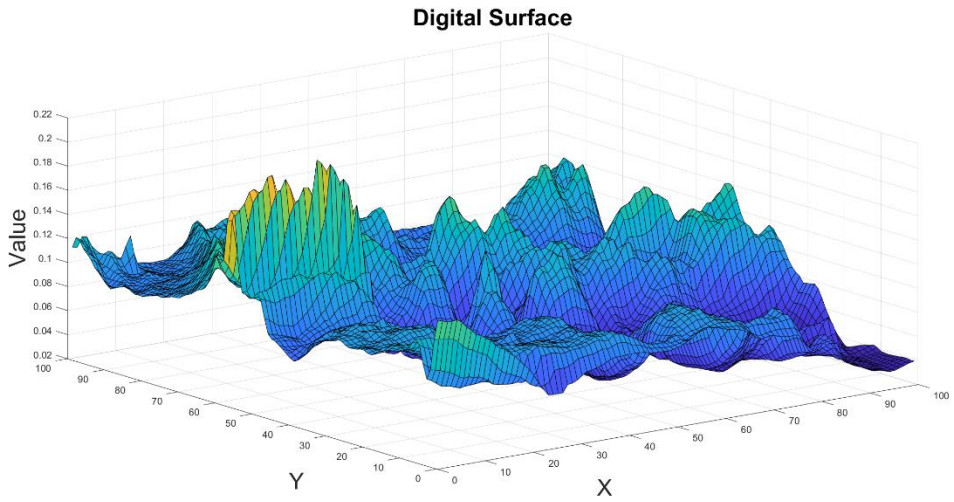

Figure 5: Digital surface of a forest stand

Smits et al. performed a study on examined local maximum algorithm to determine individual tree positions from the imagery that was sensed from aerial photography camera. They reported 71.3% of the trees were correctly identified [36]. Another study that utilized the local peak detection algorithm is performed by Srestasathiern and Rakwatin. Their study aims to detect oil palm trees from multispectral satellite imagery. They detected the location of oil palm tree by using local peak within the oil

palm tree area. F-measure values of their proposed method is ranging from 0.897 to 0.993 for different areas [13]. Khalid et al. utilized the local maxima detection for locating the trees in Ampang Forest Reserve. They reported usage of local maxima with multiresolution image segmentation detects tree positions accurately [37].

In the proposed method, I validated candidate treetops detected by local maxima detection using their shadows. Consequently, I searched for a shadow detection algorithm for detecting shadows on multispectral imagery.

2.1.4 Shadow Detection on Multispectral Image

Tsai suggested an approach for detecting shadows in color aerial images. He transformed the RGB images to different invariant color spaces. Then several ratios are proposed for these transformed images and some thresholds are applied for identifying shadowy areas. They reported that hue, saturation, and intensity (HSI); luma, inphase, and quadrature(YIQ); and YC_bC_r color models produced better results [38].

Khekade and Bhoyar carried out a study on detection of shadows in color aerial images based on RGB and YIQ color spaces. They proposed a development on study of Tsai by adding a three step post processing method including histogram equalization, box filtering and thresholding using Otsu's method. Their study showed that proposed method produces better visual performance [39].

Sevim also utilized several color spaces for detecting shadowed areas on WorldView-2 imagery [40]. To utilize the additional bands WorldView-2 provides, she also transferred false color images including the NIR bands into different color spaces. She converted RGB color space to NIR2-R-G color space. Sevim reported that improved results are obtained by using false color images on YUV and YIQ color spaces. Also, using new NIR band of WorldView-2 imagery, (NIR2), yields improved accuracy [40]. Sevim also investigated false color images on $C_1C_2C_3$ color space for detecting shadows. However, this color space did not produced satisfying results in this study [41].

Previous research has guided us in detecting tree crowns in multispectral imagery. In next chapter, the study area and proposed methodology is presented.

CHAPTER 3

METHODOLOGY

In this research, I investigated the effects of vegetation indices and shadow based validated local maxima detection algorithm for detecting tree crowns from very high resolution multispectral imagery. Some cropped scenes of WorldView-2 and Worldiew-3 multispectral images were used to evaluate the performance of the proposed method. Detailed information about the data is presented in Section 3.1. Since, some changes are occurred through the time the ground truth data was extracted from the scenes visually.

Multispectral data has often lower spatial resolution compared to panchromatic data. For this reason, data fusion via pan-sharpening was used to increase the spatial resolution of multispectral data. Pan-sharpening is described in Section 3.2. Thirteen different vegetation indices were tried that were described in Chapter 2. Novel vegetation indices are introduced and compared their performances. Also, combinations of these vegetation indices were examined for better performance. All of the vegetation indices are described in Section 3.3.

The effects of usage of Gaussian Filter with different spread value, window size and selection of spectral bands before applying local maxima detection algorithm were also examined to achieve more accurate results. Details of this method are described in Section 3.4.

Moreover, detected local peaks were validated according to shadowed areas around the peak. Removal of false detections in non-tree areas was aimed in this step. Details of the method of treetop validation based on shadows are defined in Section 3.5.

The overall tree crown detection process flowchart is presented in Figure 6.

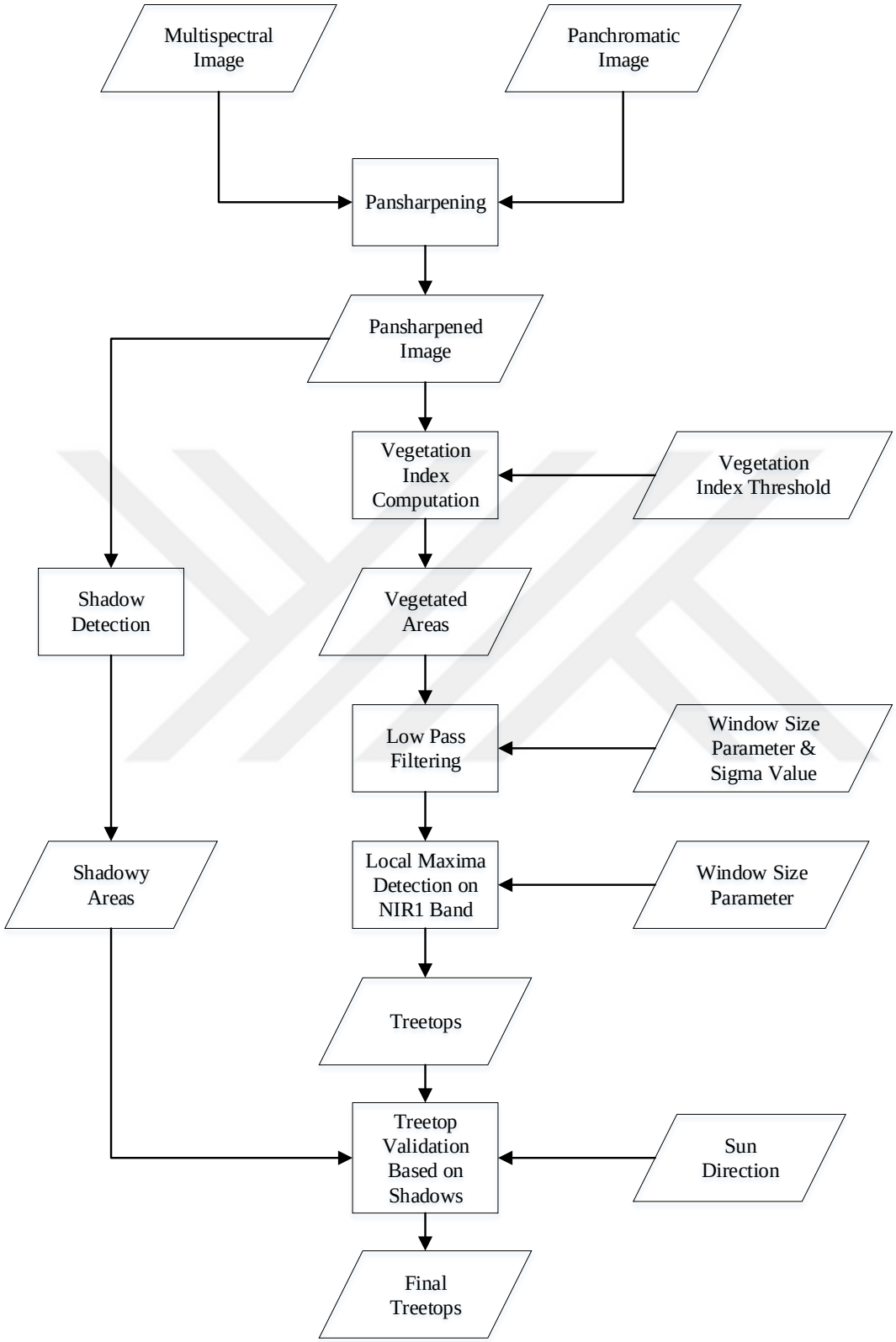

Figure 6: Flowchart of tree crown detection process

3.1 Data

In this study, WorldView-2 and Worldiew-3 multispectral images are used. Test Scene-1, Scene-2, Scene-3 and Scene-4 are acquired by WorldView-2 sensor. Scene-5, Scene-6 and Scene-7 are acquired by WorldView-3 sensor.

3.1.1 WorldView-2

The WorldView-2 sensor was launched on October 8, 2009 and owned by DigitalGlobe, Inc., USA. The WorldView-2 data includes a high spatial resolution panchromatic band and eight multispectral bands. These multispectral bands consist of coastal, blue, green, yellow, red, red edge, near-infrared 1 and near-infrared 2 with approximate spatial resolution of 2 meters. As for the panchromatic band, it provides about 0.5 meters spatial resolution. The spectral ranges of bands are listed in Table 1. The WorldView-2 image that is used in this study was acquired on November 18, 2010 (09:54Z). Pan-sharpened WorldView-2 imagery used in this study centered at 39°53'41.4"N, 32°47'02.5"E.

Table 1: Spectral bands of WorldView-2

Spectral Band	Wavelength (nm)
Panchromatic	450-800
Coastal	400-450
Blue	450-510
Green	510-580
Yellow	585-625
Red	630-690
Red Edge	705-745
Near Infrared 1	770-795
Near Infrared 2	860-1040

3.1.2 WorldView-3

The WorldView-3 sensor was launched on August 13, 2014 and owned by DigitalGlobe, Inc., USA. The WorldView-2 and WorldView-3 data includes same multispectral bands with same spectral ranges in the VNIR bands. However, the WorldView-3 data provides 0.31 meters panchromatic resolution and 1.2 meters multispectral resolution. On the other hand, WorldView-3 sensor provides eight new SWIR bands as listed in Table 2. These new bands yield 7.5 meters spatial resolution. These new SWIR bands are not utilized in this research. The WorldView-3 image that is used in this study was acquired on July 16, 2016 (08:58Z). Pan-sharpened WorldView-3 imagery used in this study centered at 39°53'41.4"N, 32°47'02.5"E.

Table 2: New spectral bands of WorldView-3

Spectral Band	Wavelength (nm)
SWIR-1	1195-1225
SWIR-2	1550-1590
SWIR-3	1640-1680
SWIR-4	1710-1750
SWIR-5	2145-2185
SWIR-6	2185-2225
SWIR-7	2235-2285
SWIR-8	2295-2365

3.1.3 Study Area

The campus of Middle East Technical University located in Ankara, Turkey, is chosen as the study area. In order to evaluate the accuracy of the proposed methods seven different scenes are selected within the WorldView-2 and WorldView-3 multispectral images. However, since acquisition time of the imageries is different, I did not prefer to select same areas for WorldView-2 and WorldView-3 multispectral images. Also, three more images are extracted from WorldView-2 and WorldView-3 imagery for visual analysis. Since ground truths do not exist for these images, detected treetops and validated treetops marked and presented for visual analysis on APPENDIX A.

3.1.3.1 Scene-1: METU Dense Forest

Scene-1 is cropped from WorldView-2 imagery and consists of 188x256 pixels. Ground truth of Scene-1 for calculating vegetation indices accuracy is created by detecting the pixels that belong to trees visually. The number of pixels belonging to trees and other areas is presented in Table 3.

Table 3: Number of pixels of ground truth for Scene-1

#	Class	Number of Pixels
1	Tree	15809
2	Other	32319

Furthermore, tree crowns that are located in Scene-1 are counted visually. According to ground truth of Scene-1, the image includes 176 tree crowns. Spectral plot of some of these tree crowns and other vegetated areas like grass are shown in Figure 7. The values of corresponding bands are the average of pixels within a 5x5 neighborhood.

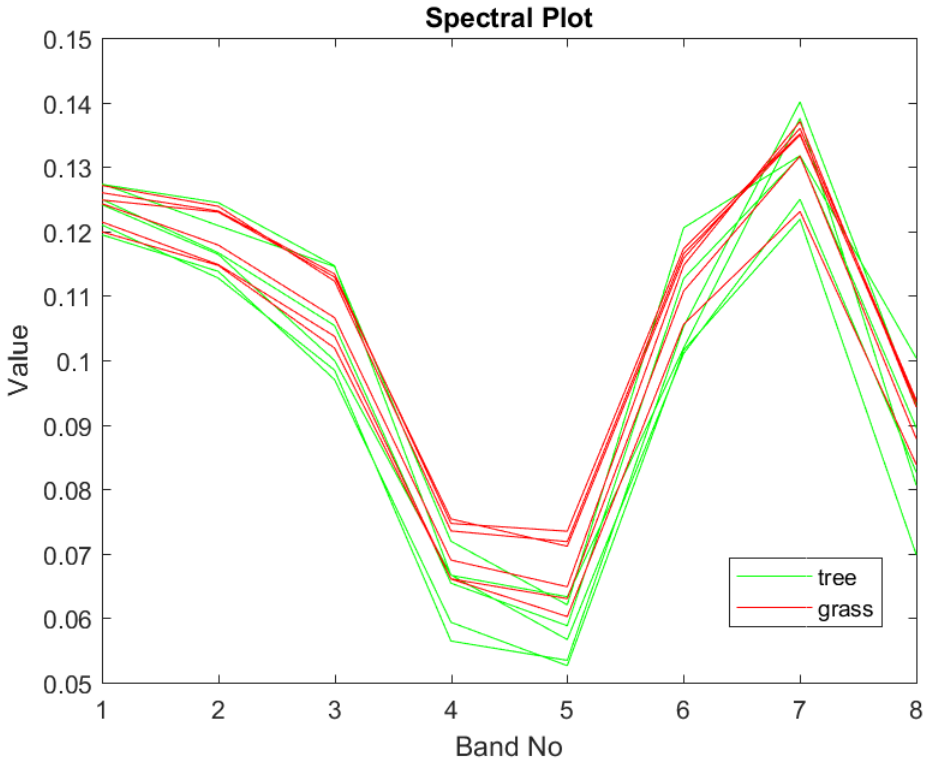

Figure 7: Spectral plot of sample trees and grass in Scene-1

The visual of Scene-1 and ground truth for it is represented in Figure 8.

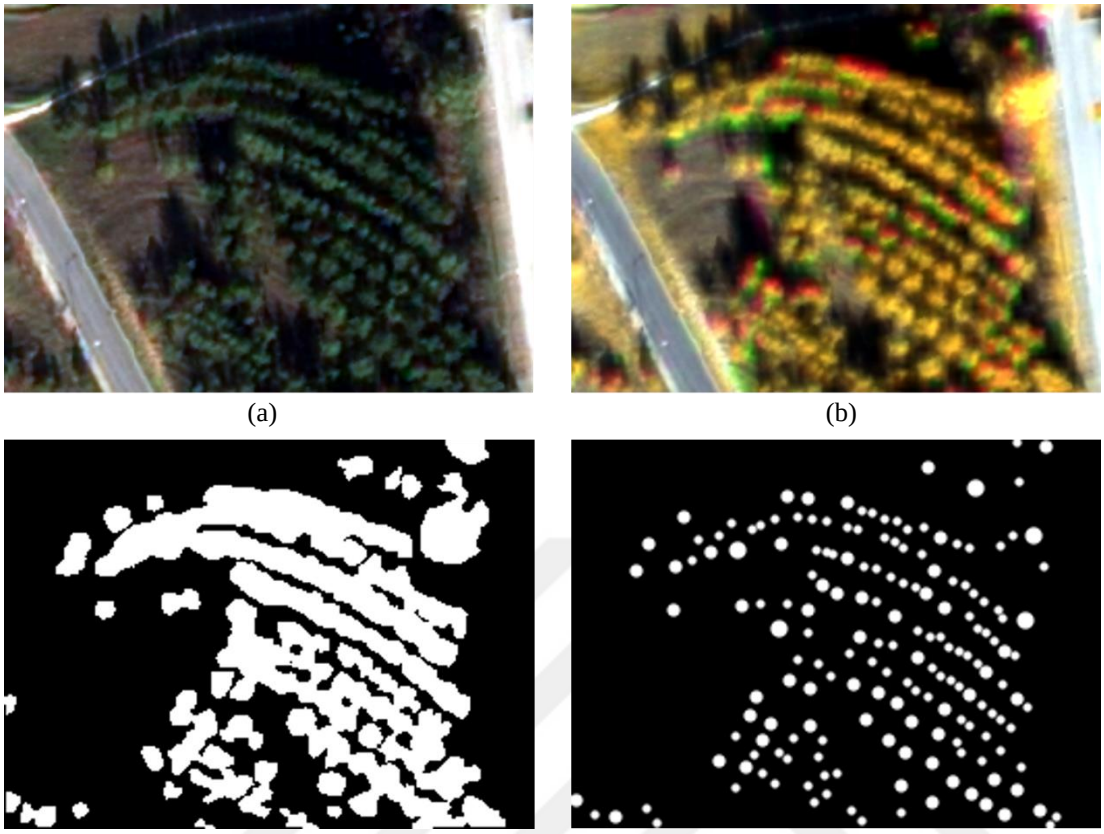

Figure 8: (a) Scene-1 RGB image (b) Scene-1 false color image (c) Ground truth image for vegetation indices (d) Ground truth image for treetops

3.1.3.2 Scene-2: METU Thin Forest

Scene-2 is also acquired by WorldView-2 multispectral sensor and consists of 352x460 pixels. Ground truth of Scene-2 created by investigating the imagery pixel by pixel for detecting the trees visually. The pixels classified into two classes; tree crowns and others. The number of pixels belonging to trees and other areas can be seen in Table 4.

Table 4: Number of pixels of ground truth for Scene-2

#	Class	Number of Pixels
1	Tree	39315
2	Other	122605

In addition to pixel based ground truth, tree crowns that are located in Scene-2 are counted visually. According to ground truth of Scene-2, the image includes 547 tree crowns. Spectral plot of some of these tree crowns and other vegetated areas like grass can be seen in Figure 9. The values of corresponding bands are the average of pixels within a 5x5 neighborhood.

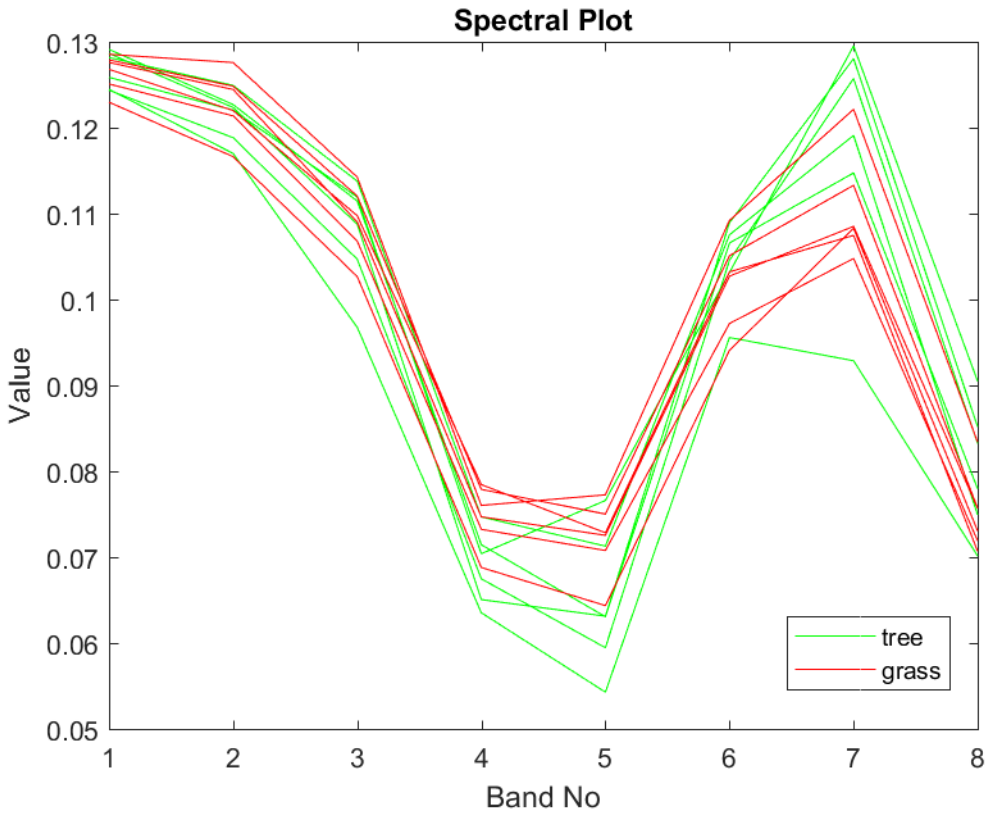

Figure 9: Spectral plot of sample trees and grass in Scene-2

Figure 10 includes the visual of Scene-2 and ground truth image of Scene-2.

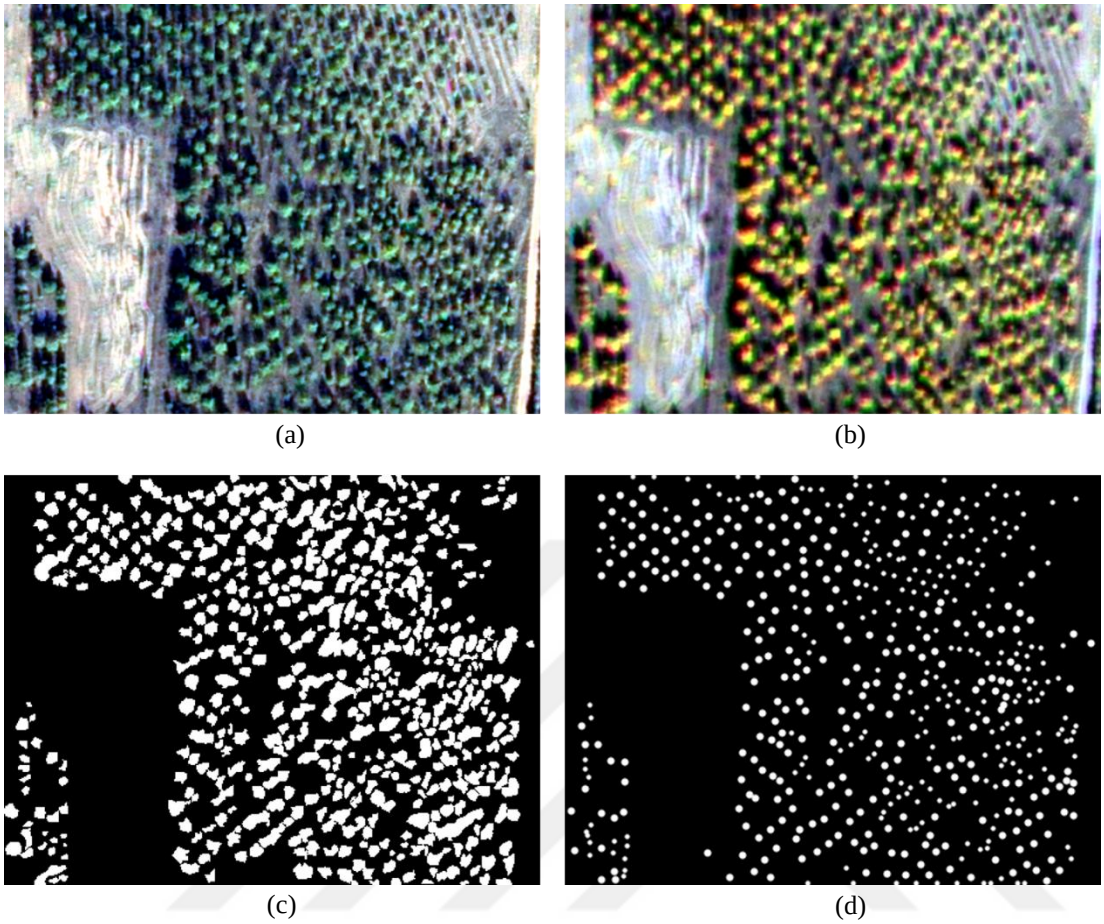

Figure 10: (a) Scene-2 RGB image (b) Scene-2 false color image (c) Ground truth image for vegetation indices (d) Ground truth image for treetops

3.1.3.3 Scene-3: METU Urban Area

Scene-3 is also acquired by WorldView-2 and consists of 260x264 pixels. Scene-3 ground truth is created by investigating the image pixel by pixel for detecting the trees visually. The pixels are classified into two classes; tree crowns and others. The number of pixels belonging to trees and other areas can be seen in Table 5.

Table 5: Number of pixels of ground truth for Scene-3

#	Class	Number of Pixels
1	Tree	11936
2	Other	56704

In addition to pixel based ground truth, tree crowns that are located in Scene-3 are counted visually. According to ground truth of Scene-3, the image includes 100 tree crowns. Spectral plot of some of these tree crowns and other vegetated areas like grass is shown in Figure 11. The values of corresponding bands are the average of pixels within a 5x5 neighborhood.

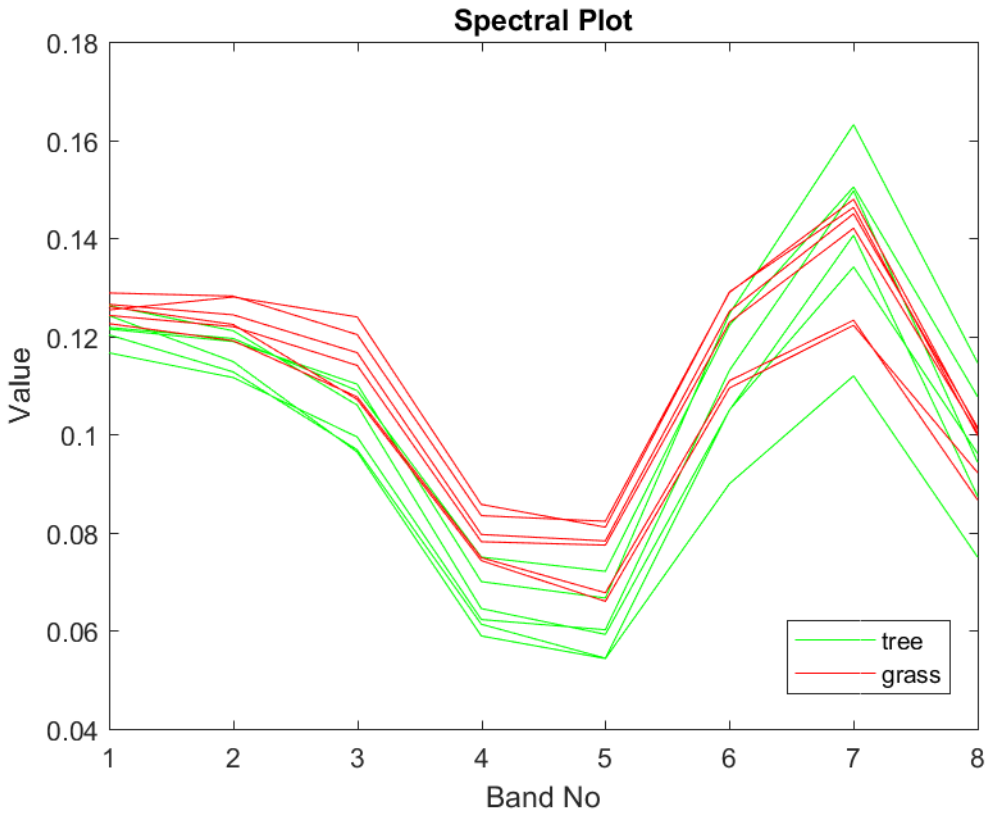

Figure 11: Spectral plot of sample trees and grass in Scene-3

Figure 12 depicts Scene-3 and its ground truth.

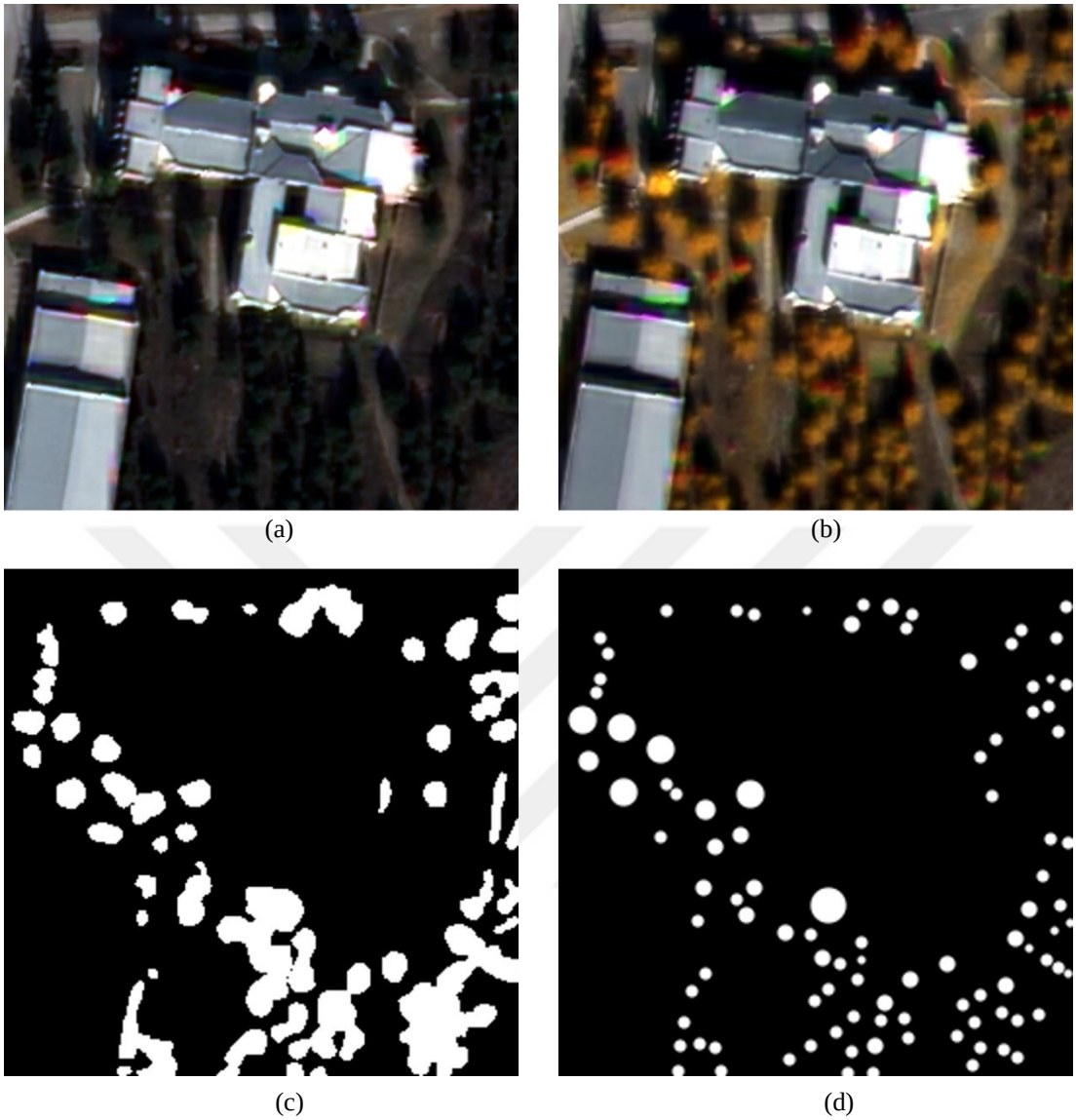

(a) (b)

(c) (d)

Figure 12: (a) Scene-3 RGB image (b) Scene-3 false color image (c) Ground truth image for vegetation indices (d) Ground truth image for treetops

3.1.3.4 Scene-4: METU Stadium

Scene-4 is also acquired by WorldView-2 and consists of 350x360 pixels. Scene-4 ground truth created by investigating the imagery pixel by pixel for detecting the trees visually. The pixels are classified into two classes; tree crowns and others. The number of pixels belonging to trees and other areas can be seen in Table 6.

Table 6: Number of pixels of ground truth for Scene-4

#	Class	Number of Pixels
1	Tree	30046
2	Other	95954

In addition to pixel based ground truth, tree crowns that are located in Scene-4 are counted visually. According to ground truth of Scene-4, the image includes 262 tree crowns. Spectral plot of some of these tree crowns and other vegetated areas like grass can be shown in Figure 13. The values of corresponding bands are the average of pixels within a 5x5 neighborhood.

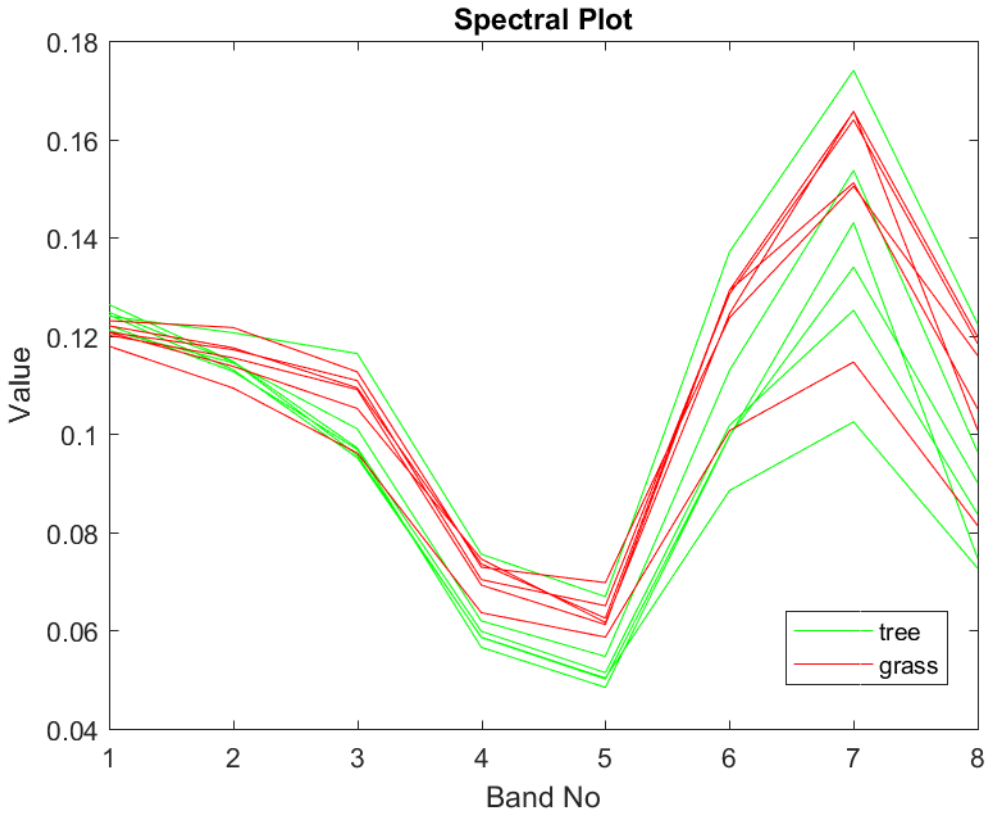

Figure 13: Spectral plot of sample trees and grass in Scene-4

Figure 14 includes the visual of Scene-4 and ground truth image of it.

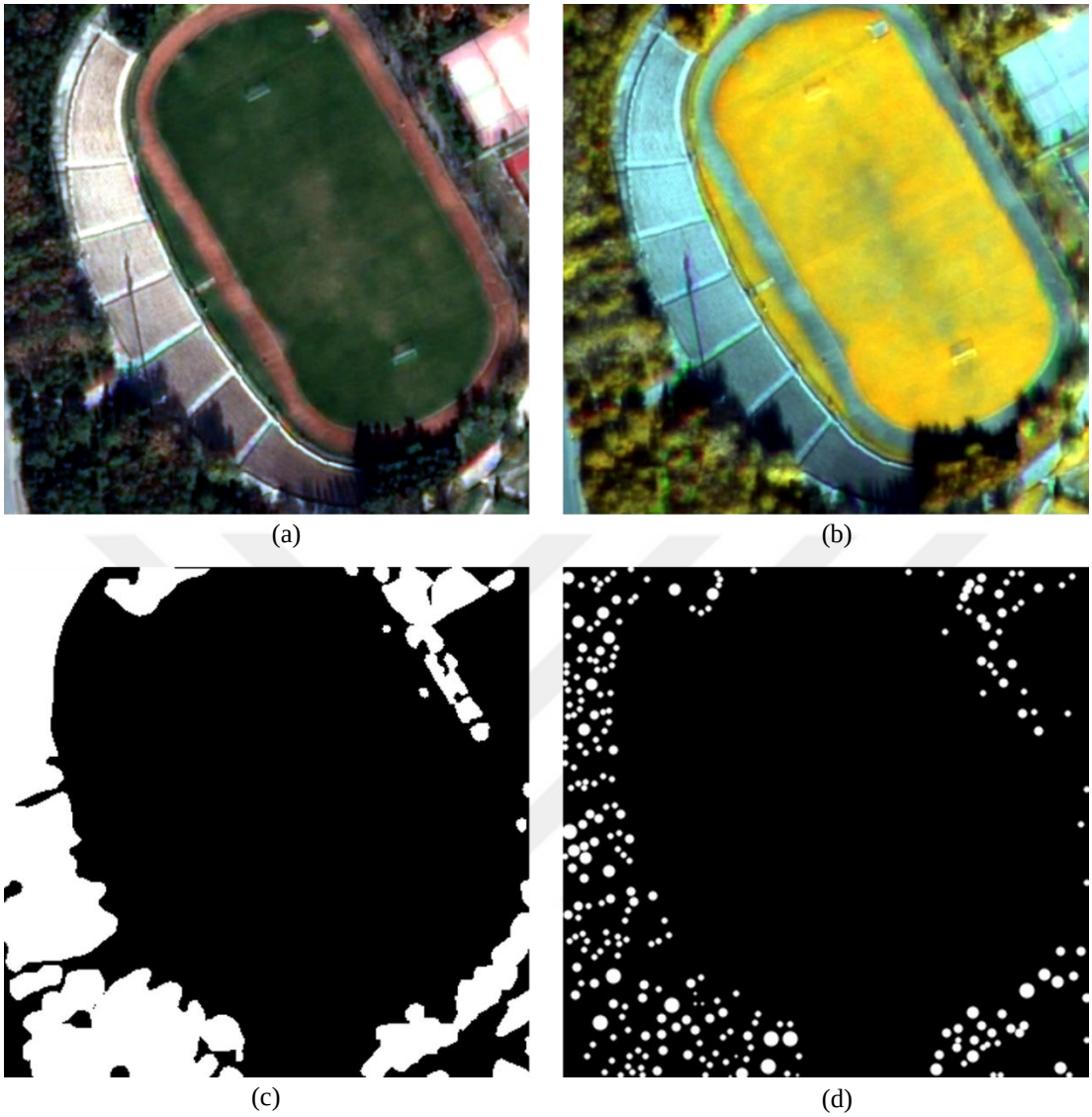

Figure 14: (a) Scene-4 RGB image (b) Scene-4 false color image (c) Ground truth image for vegetation indices (d) Ground truth image for treetops

3.1.3.5 Scene-5: METU Regular Forest

Scene-5 is acquired by WorldView-3 multispectral sensor and consists of 228x271 pixels. Scene-5 ground truth created by investigating the imagery pixel by pixel for detecting the trees visually. The pixels classified into two classes; tree crowns and others. The number of pixels belonging to trees and other areas are listed in Table 7.

Table 7: Number of pixels of ground truth for Scene-5

#	Class	Number of Pixels
1	Tree	11791
2	Other	49997

In addition to pixel based ground truth, tree crowns that are located in Scene-5 are counted visually. According to ground truth of Scene-5, the image includes 163 tree crowns. Spectral plot of some of these tree crowns and other vegetated areas like grass can be shown in Figure 15. The values of corresponding bands are the average of pixels within a 5x5 neighborhood.

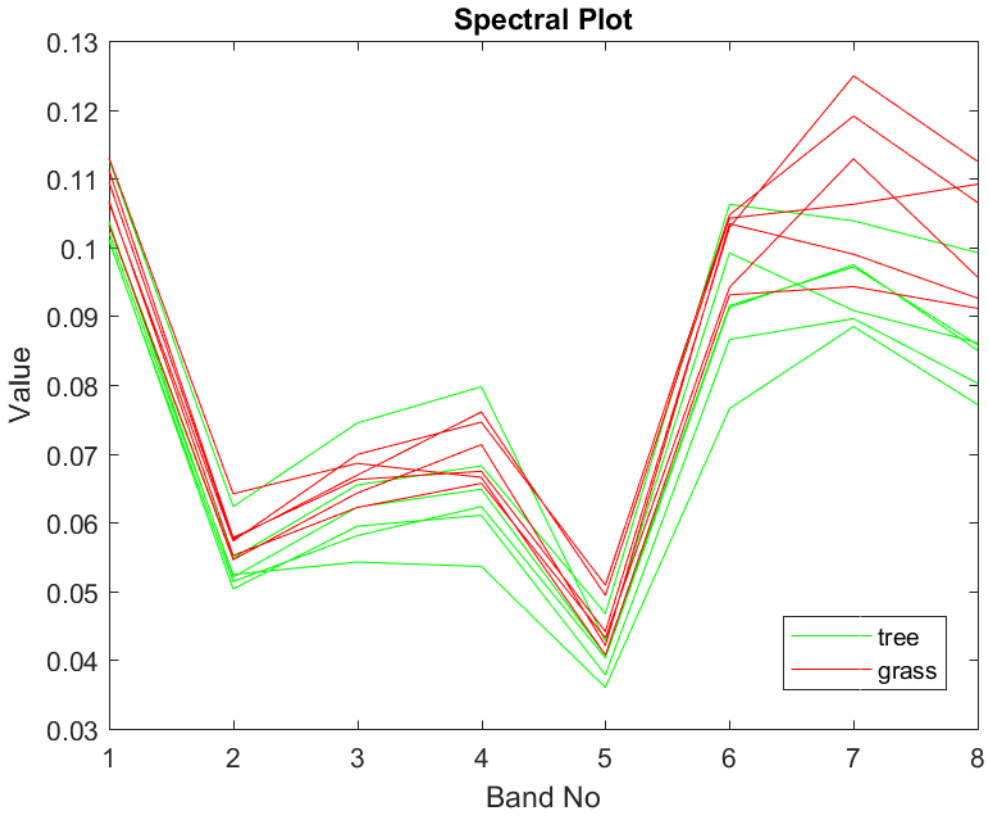

Figure 15: Spectral plot of sample trees and grass in Scene-5

Figure 16 depicts Scene-5 and ground truth of it.

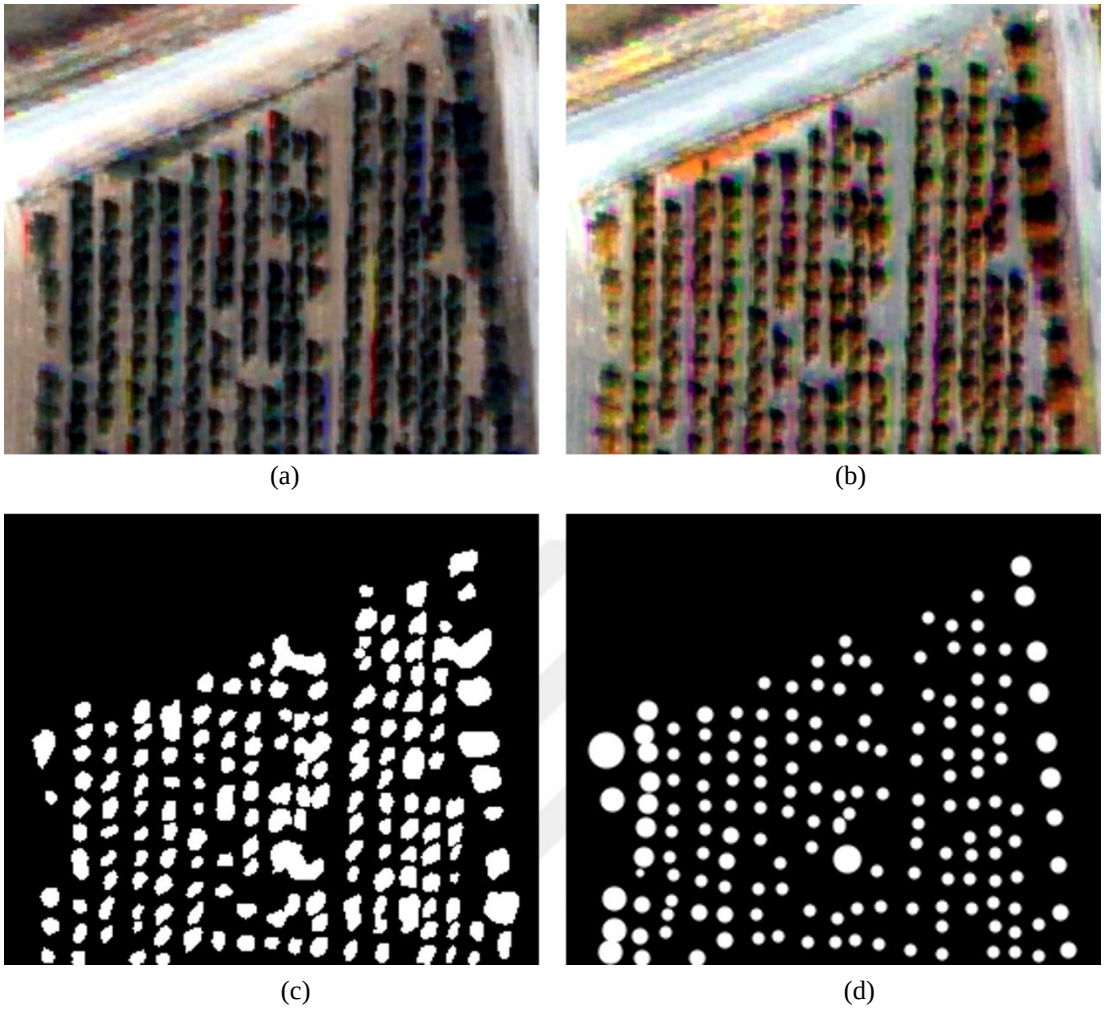

(a) (b)

(c) (d)

Figure 16: (a) Scene-5 RGB image (b) Scene-5 false color image (c) Ground truth image for vegetation indices (d) Ground truth image for treetops

3.1.3.6 Scene-6: METU Urban Area

Scene-6 is also acquired by WorldView-3 multispectral sensor and consists of 312x376 pixels. Scene-6 ground truth created by investigating the imagery pixel by pixel for detecting the trees visually. The pixels classified into two classes; tree crowns and others. The number of pixels belonging to trees and other areas can be seen in Table 8.

Table 8: Number of pixels of ground truth for Scene-6

#	Class	Number of Pixels
1	Tree	37607
2	Other	79705

In addition to pixel based ground truth, tree crowns that are located in Scene-6 are counted visually. According to ground truth of Scene-6, the image includes 64 tree crowns. Spectral plot of some of these tree crowns and other vegetated areas like grass can be shown in Figure 17. The values of corresponding bands are the average of pixels within a 5x5 neighborhood.

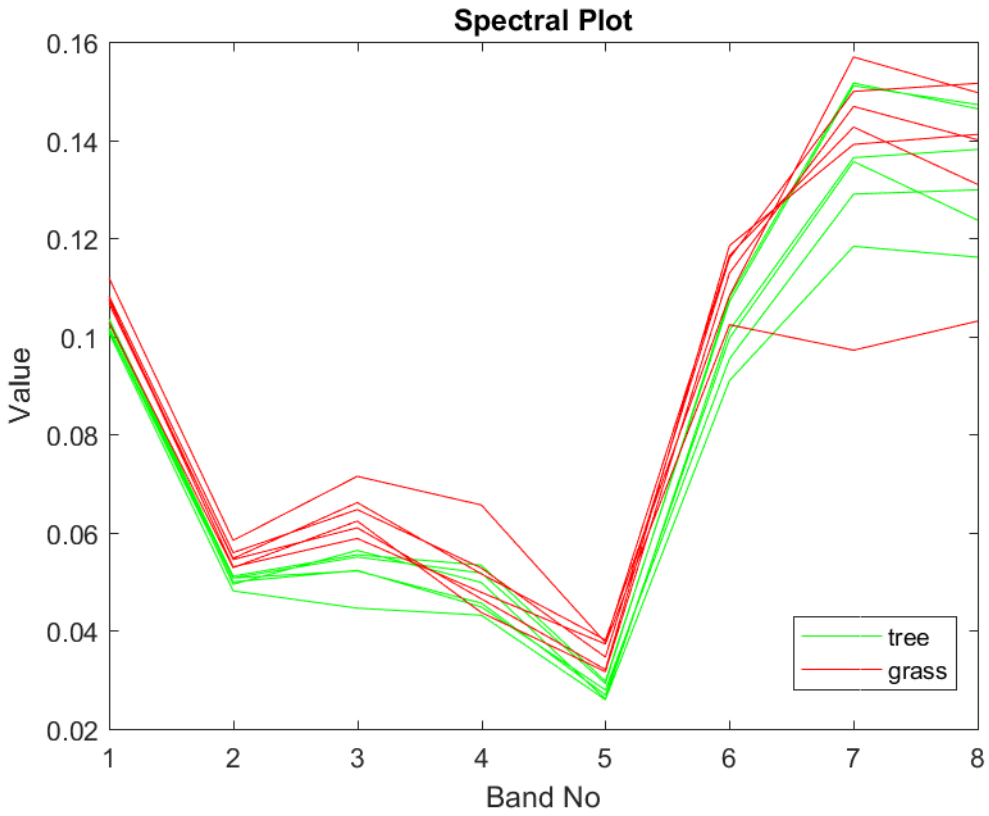

Figure 17: Spectral plot of sample trees and grass in Scene-6

Figure 18 includes the visual and ground truth image of Scene-6.

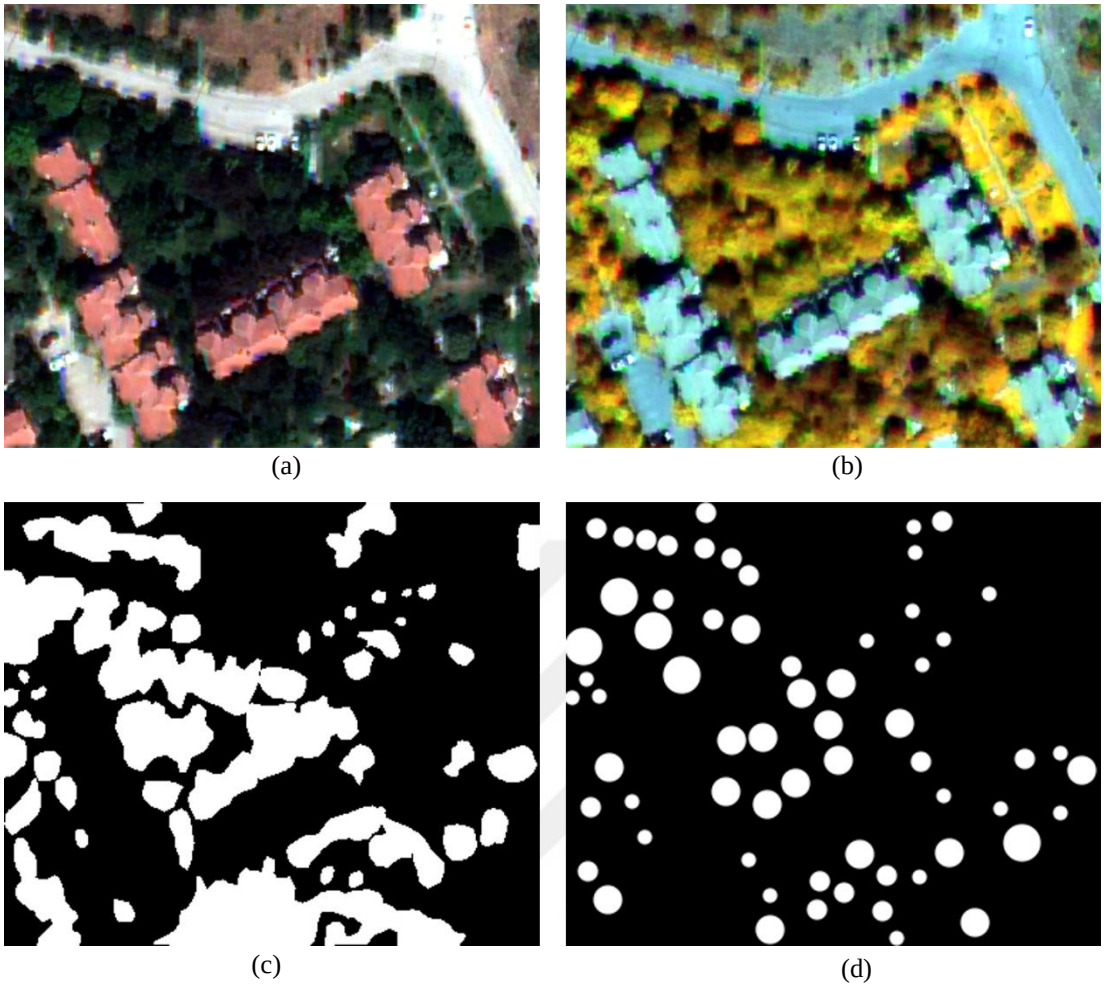

Figure 18: (a) Scene-6 RGB image (b) Scene-6 false color image (c) Ground truth image for vegetation indices (d) Ground truth image for treetops

3.1.3.7 Scene-7: Urban Area

Scene-7 is acquired by WorldView-3 multispectral sensor and consists of 548x965 pixels. Scene-7 ground truth created by investigating the imagery pixel by pixel for detecting the trees visually. The pixels classified into two classes; tree crowns and others. The number of pixels belonging to trees and other areas are represented in Table 9.

Table 9: Number of pixels of ground truth for Scene-7

#	Class	Number of Pixels
1	Tree	85519
2	Other	444301

In addition to pixel based ground truth, tree crowns that are located in Scene-7 are counted visually. According to ground truth of Scene-7, the image includes 171 tree crowns. Spectral plot of some of these tree crowns and other vegetated areas like grass can be shown in Figure 19. The values of corresponding bands are the average of pixels within a 5x5 neighborhood.

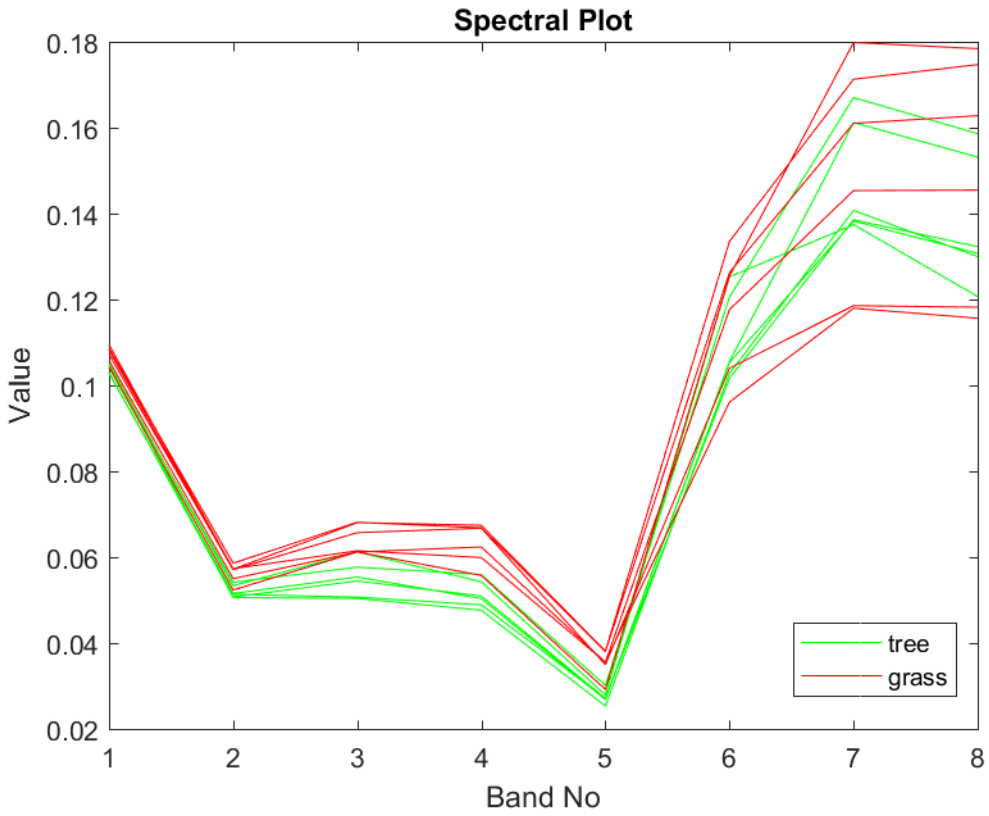

Figure 19: Spectral plot of sample trees and grass in Scene-7

Figure 20 includes the visual of Scene-7 and ground truth image for Scene-7.

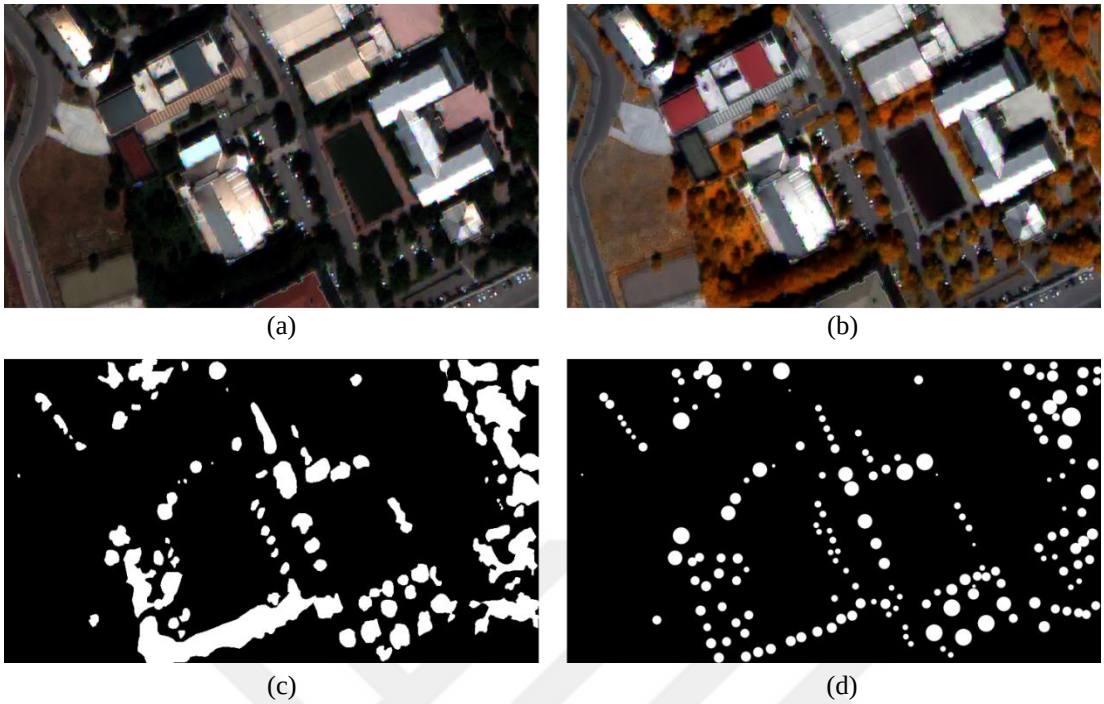

Figure 20: (a) Scene-7 RGB image (b) Scene-7 false color image (c) Ground truth image for vegetation indices (d) Ground truth image for treetops

3.2 Preprocessing with HCS Pan-Sharpening

The spatial resolution of multispectral imagery is increased by using a new pan-sharpening method that is called Hyperspherical Color Sharpening (HCS). Although naïve mode of HCS is easy to implement, it causes some color distortion in the pan-sharpened image. However, Padwick et al. reported smart mode of HCS did show acceptable performance of imitating the original colors of multispectral image [7]. Thus, I utilized smart mode of HCS algorithm in this study. In smart mode, firstly panchromatic band is smoothed using sliding window convolution filter. This filter is applied with a 7x7 square window. In this window output value of center pixel is the mean of all pixel values in the 7x7 neighborhood. Smoothed version of the panchromatic band is formed as follows:

$$Pan_{smooth} = SMOOTH(Pan) \tag{16}$$

Next, the square of the multispectral intensity (I^2), the square of the panchromatic intensity (P^2) and the square of the smoothed version of the panchromatic band (PS^2) are computed, as given in Equations 17-19. X_i denotes the i^{th} spectral band of the multispectral image.

$$I^2 = \sum_{i=1}^{n} X_i^2 \tag{17}$$

$$P^2 = (Pan)^2 \tag{18}$$

$$PS^2 = (Pan_{smooth})^2 \tag{19}$$

Next, transformation of native color space to the hyperspherical color space is performed. For an image having *n* input bands, one forms a single intensity component and *n-1* angles on the hypersphere. Equations 20-23 give the transformation into HCS from an *n*-band color space:

$$I = \sqrt{X_1^2 + X_2^2 + \cdots + X_n^2} \tag{20}$$

$$\varphi_1 = tan^{-1}\left(\frac{\sqrt{X_n^2 + X_{n-1}^2 + \cdots + X_2^2}}{X_1}\right) \tag{21}$$

$$\varphi_{n-2} = tan^{-1}\left(\frac{\sqrt{X_n^2 + X_{n-1}^2}}{X_{n-2}}\right) \tag{22}$$

$$\varphi_{n-1} = tan^{-1}\left(\frac{X_n}{X_{n-1}}\right) \tag{23}$$

In the transformation, the angular (φ_n) variables describe the color or hue, the radial (I) part describes the intensity of the color.

Next, the algorithm intensity matches both PS^2 and P^2 signal to the I^2 signal using the Equations 24-25. In this equation μ_0 and σ_0 represent mean and standard deviation of I^2, μ_1 and σ_1 represent mean and standard deviation of PS^2.

$$PS^2 = \frac{\sigma_0}{\sigma_1}(PS^2 - \mu_1 + \sigma_1) + \mu_0 - \sigma_0 \quad (24)$$

$$P^2 = \frac{\sigma_0}{\sigma_1}(P^2 - \mu_1 + \sigma_1) + \mu_0 - \sigma_0 \quad (25)$$

The adjusted intensity is given by the Equation 26 where the I_{adj} is the pan-sharpened intensity.

$$I_{adj} = \sqrt{\frac{P^2}{PS^2} I^2} \quad (26)$$

Finally, the pan-sharpened intensity is transformed back into the original color space as:

$$X_1 = I_{adj} \cos \varphi_1 \quad (27)$$

$$X_2 = I_{adj} \sin \varphi_1 \cos \varphi_2 \quad (28)$$

$$X_{n-1} = I_{adj} \sin \varphi_1 \sin \varphi_2 \dots \sin \varphi_{n-2} \cos \varphi_{n-1} \quad (29)$$

$$X_n = I_{adj} \sin \varphi_1 \sin \varphi_2 \dots \sin \varphi_{n-2} \sin \varphi_{n-1} \quad (30)$$

I employed ERDAS Imagine 2015 built in HCS function with 7x7 pixel smoothing filter in this study. The original multispectral image and pan-sharpened image can be seen in Figure 21 in RGB color space.

(a)

(b)

(c)

Figure 21: (a) Original WorldView-2 PAN image (b) Original WorldView-2 MS image (c) HCS sharpened image

The spectral plot of sample pixel of original multispectral imagery and the corresponding pixels of pan-sharpened multispectral imagery are depicted in Figure 22.

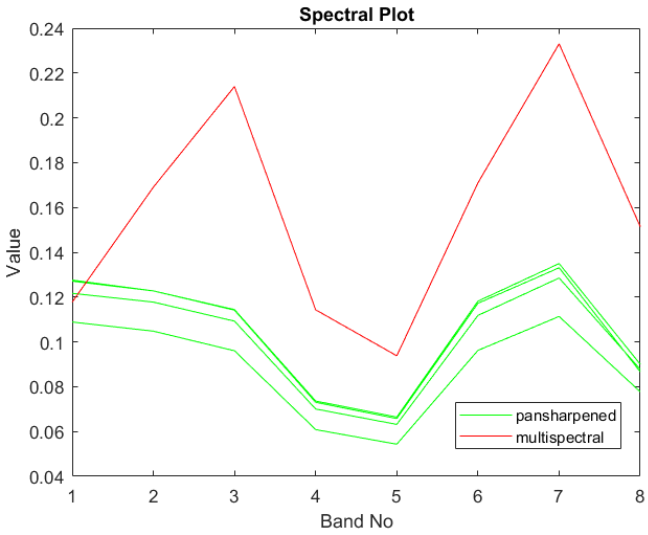

Figure 22: Spectral plot of sample pixels of original and pan-sharpened multispectral imagery

3.3 Vegetation Indices

In the context of this study, masking non vegetated areas by applying vegetation index threshold is suggested by many researchers. While Mei and Durrieu utilized the NDVI for identifying non-vegetated areas [42], Perez et al. used NDI for detecting weed [18]. In this method, firstly, the vegetation index is calculated by using pixel values in different spectral bands. After vegetation index matrix created a threshold is defined for masking out the non-vegetated area. This threshold value can be calculated experimentally. For example, Daliakopoulos et al. revealed 0.37 as NDVI threshold produced better accuracy for selected sample area, but in different scenes this threshold value has not worked well and needed to be changed [1]. I examined different threshold values for different scenes. The best threshold value is searched in steps of 0.01 within the range of minimum and maximum values of the vegetation index. The flowchart of finding best threshold value for a vegetation index can be shown in Figure 23.

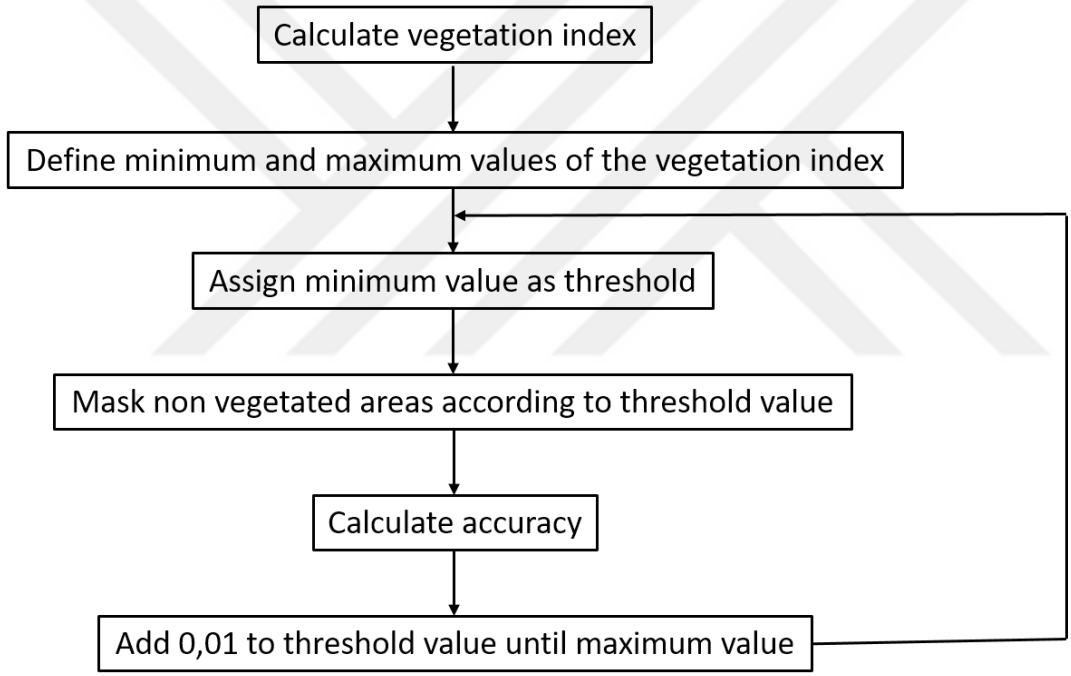

Figure 23: Flowchart of vegetation index threshold detection

After detecting the best threshold value for the vegetation index, non-vegetated areas are masked out in the image. Consequently, masking the image by thresholding vegetation indices produced non vegetated area free image for detecting tree crown. The created image after masking out the non-vegetated areas for scene-1 is shown in Figure 24.

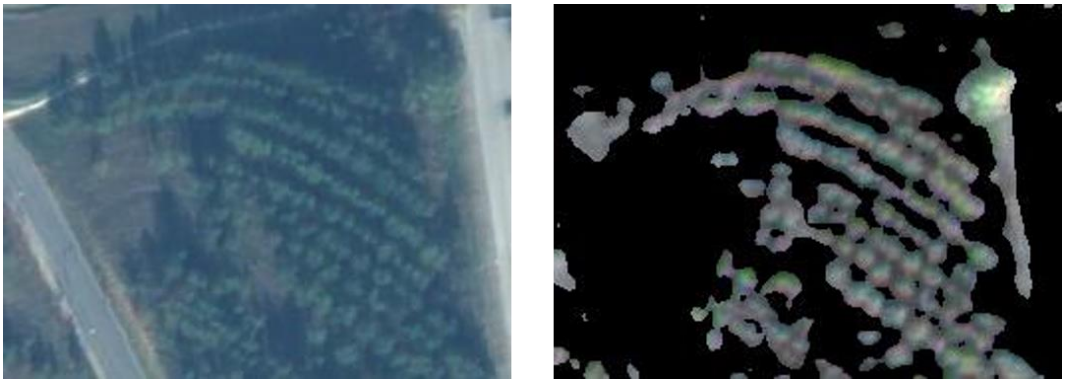

(a) (b)

Figure 24: (a) Original WorldView-2 PAN image (b) Masked image with NDVI1

It can be seen in Figure 24 that vegetation indices detect vegetated areas. However, these areas contain not only tree crowns, but also grass. This is a challenge for detecting tree crowns. Because, some areas that do not contain tree crown can be detected as tree crown in local maxima method. Thus, I try to find the best vegetation index or combination of vegetation indices that does not detect the grass or other areas that does not contain tree crown. Figure 25 shows spectral plot of a pixel that belongs to a tree crown and a pixel that belongs to grass.

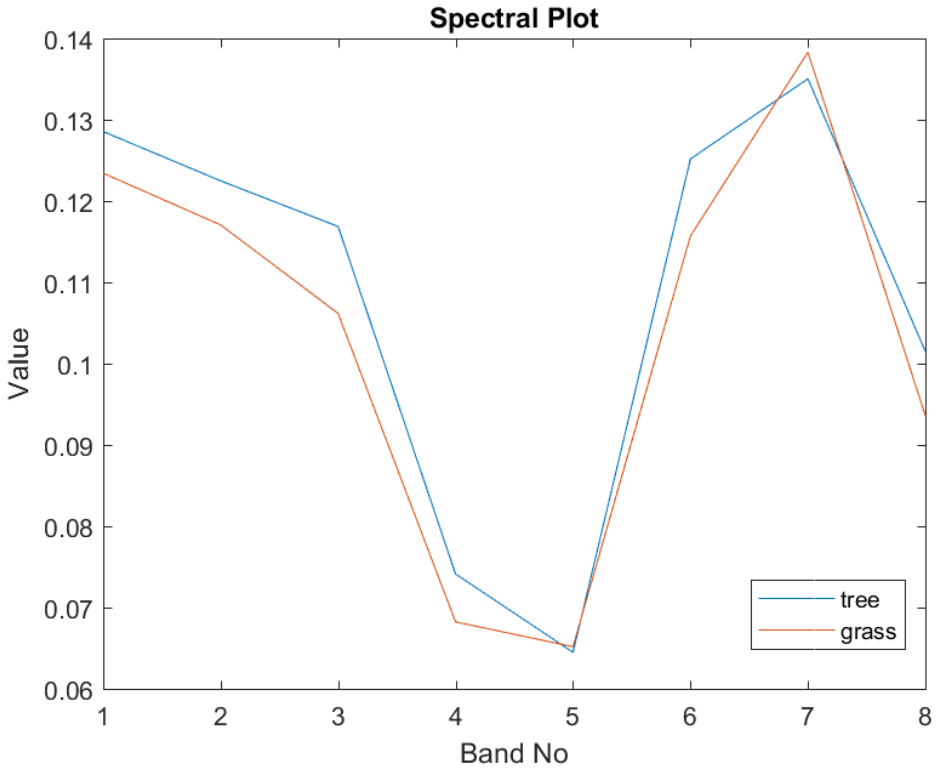

Figure 25: Spectral plot of tree and grass pixel

Spectral signature of grass and tree crown is almost same as can be seen in Figure 25. So, the issue of discriminating grass and tree crowns using vegetation indices is difficult. For this reason, potential of various vegetation indices are investigated using different threshold values.

The pre-defined vegetation indices and their calculation formulas can be seen in Table 10.

Table 10: Pre-defined vegetation indices

	Vegetation Index	Formula
1	Excess Green[1]	2g - r -b
2	Excess Red[2]	1.4r - g
3	Excess Blue[3]	1.4b - g
4	Excess Green - Excess Red	Excess Green - Excess Red
5	Normalized Difference Index	(G - R) / (G + R)
6	Green Normalized Difference Vegetation Index	(NIR1 - G) / (NIR1 + G)
7	NIR2-yellow ratio	(NIR2 - Y) / (NIR2 + Y)
8	RedEdge yellow ratio	(RE - Y) / (RE + Y)
9	NIR-Red-yellow ratio	(NIR1) / (R + Y)
10	Normalized Red	R / (NIR1 + R + G)
11	Normalized NIR	NIR1 / (NIR1 + R + G)
12	Normalized Difference Vegetation Index-1	(NIR1 - R) / (NIR1 + R)
13	Normalized Difference Vegetation Index-2	(NIR2 - R) / (NIR2 + R)

In addition to predefined vegetation indices, combinations of these indices are examined for better results. For double combination, after applying threshold to vegetation indices, if both vegetation indexes vote a pixel as vegetated area, the pixel is taken as vegetated area. Otherwise, the pixel is taken as non-vegetated area.

At the same time, ratios of spectral bands, ratio of one spectral band to sum of two spectral bands and ratio of one spectral band to sum of three spectral bands is calculated for creating vegetation indices. Also, some self-developed vegetation indices are calculated to get better results. I changed the spectral bands of excess green, excess red, excess blue vegetation index with red, red edge and near infrared-1 bands of WorldView-2 multispectral imagery to get new vegetation indices. The self-developed vegetation indices and their formulas of them can be seen in Table 11.

---

[1] g = G / (R + G + B)

[2] r = R / (R + G + B)

[3] b = B / (R + G + B)

Table 11: Self-developed vegetation indices

	Vegetation Index	Formula
1	index1	2nir - re - r
2	index2	2.5nir - re - r
3	index3	1.4re - nir
4	index4	1.74r - nir
5	index5	nir - r
6	index6	2nir - 1.4r
7	index7	nir – re
8	index8	(((2NIR1 + NIR2) / 3) - R) / (((2NIR1 + NIR2) / 3) + R)

Nir, re, and r components of indices 1-7 are computed as:

$$nir = NIR1 / (NIR1 + RE + R) \quad (31)$$

$$re = RE / (NIR1 + RE + R) \quad (32)$$

$$r = R / (NIR1 + RE + R) \quad (33)$$

3.4 Local Maxima Detection

Local maxima detection method seeks local maximum pixels in windows. However, applying this method to masked image directly can result some false detections. Since some local peaks are located at flat-topped area, these peaks cannot be detected by this method. So, many researchers utilized Gaussian filter for overcoming this challenge. Applying Gaussian low pass filter also reduces the multiple peaks in the local area.

The Gaussian low filter is defined in 2-D as given below and the distribution is shown in Figure 26.

$$G(x, y) = \frac{1}{2\pi\sigma^2} e^{-\frac{x^2+y^2}{2\sigma^2}} \quad (34)$$

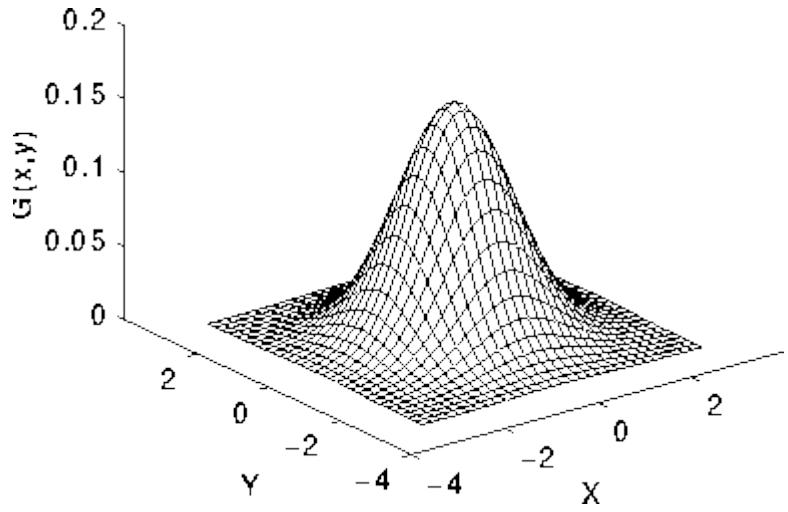

Figure 26: 2-D Gaussian Distrubiton

The Gaussian filter is examined with different window size and sigma values. In this filter, sigma value corresponds to blurring effect. Higher sigma values result more blurred image. On the other hand, window size has an effect on blurring with correct pixels.

After applying the Gaussian filter to the image, local maxima detection algorithm runs for detecting treetops as local peaks. This algorithm traces peaks in local areas that is defined as (2n+1) x (2n+1) windows. The parameter n is estimated as average size of trees in the image. This parameter is most important parameter for local maxima detection algorithm. If the parameter n is too large, the local area will include too many local peaks.

The local maxima detection algorithm works as sliding window. It compares the center pixel with other pixels within the window and if the center pixel has higher brightness value than the other pixels, it marks the center pixel as local peak. However, if the window has a pixel that has higher brightness value than the center pixel it passes to other pixel and seeks neighbor pixels within the window again. Hereby, the local maxima detection algorithm seeks all pixels image except that n pixels in the edges of image.

The overall flow of local maxima detection algorithm as follows;

- For each pixel;
- Go to first pixel of image which is not belongs to n pixels in the edges of image.
- Initialize coordinate (x, y).
- Define the neighbor pixels within (2n+1) x (2n+1) pixels.
- Compare the brightness value of the pixel with the other pixels in the window.

- If there is no pixel that has higher brightness value than main pixel, mark the pixel as local peak.
- If there is a pixel that has higher brightness value than main pixel, pass to the next pixel.

After of local maxima detecion algorithm runs, detected treetops in scene-1 can be seen in Figure 27.

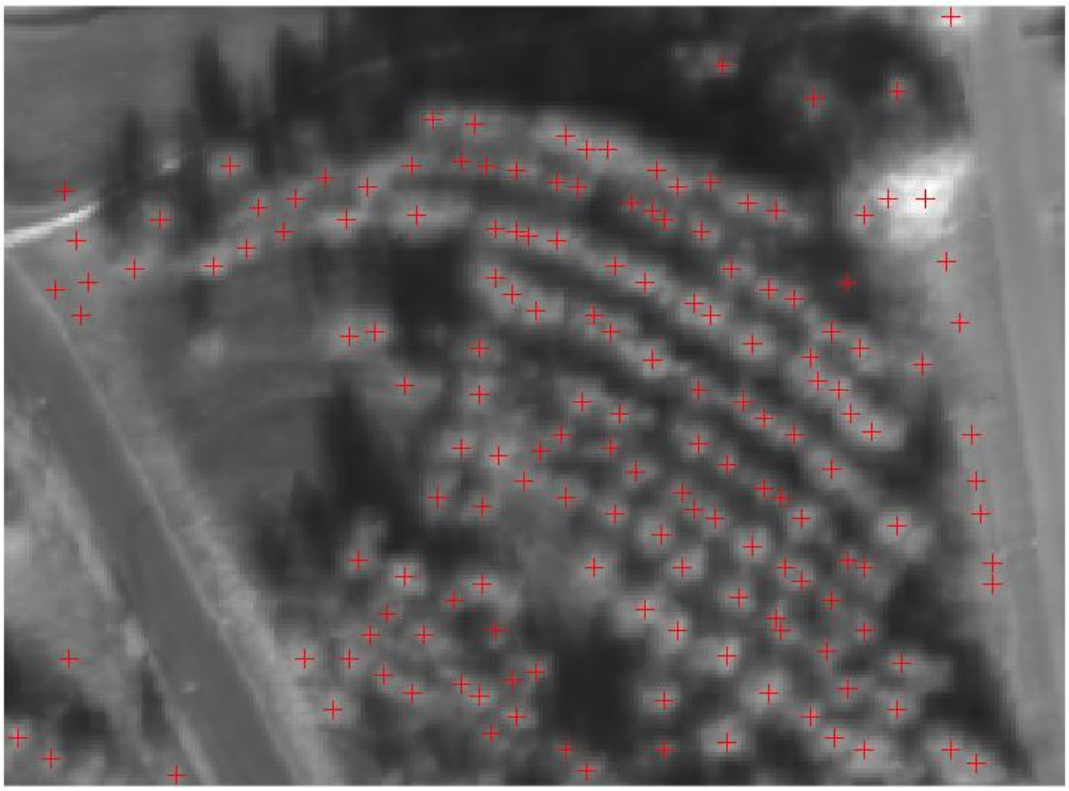

Figure 27: Detected treetops in Scene-1

3.5 Treetop Validation Based on Shadows

In the final step of proposed method, I tracked shadowed pixels on the image for removing false detections that actually belong to non-tree area. The main idea of this step is based on the fact that there should be a shadowy area if there is no other high object like a tree or building in the vicinity of the tree. Ok proposed a novel methodology to detect buildings from multispectral imagery in this manner [43]. Consequently, I tracked the shadowy areas to validate the detected treetops.

For this step, firstly, I utilized shadow detection method based on YIQ color space to detect shadowed areas. In first step of this method, RGB color space was transformed to YIQ color space according to the conversion given below [40]:

$$\begin{bmatrix} Y \\ I \\ Q \end{bmatrix} = \begin{bmatrix} 0.299 & 0.587 & 0.114 \\ 0.596 & -0.274 & -0.322 \\ 0.211 & -0.523 & 0.312 \end{bmatrix} \begin{bmatrix} R \\ G \\ B \end{bmatrix} \quad (35)$$

In this study, false color image formed by using Green, Red and NIR2 bands was used as input image of YIQ transformation. Since both I and Q components of YIQ color space have low values on shadowy pixels of false color images, the following ratio is proposed:

$$Ratio = \frac{Y - \min(Y)}{\max(Y) - \min(Y)} \quad (36)$$

After calculating the ratio, automatic threshold point is calculated according to Otsu's method [44]. In this method the assumption that every scene includes shadowed areas, is made. In this step, Otsu's method is applied twice. First, the method is applied for detecting candidate shadowed areas. Then, it is applied for a second time to candidate shadowy pixels for detecting final shadowy pixels. First and second threshold values produced by Otsu's method for each scene is listed in Table 12.

Table 12: Threshold values for each scene

	First Threshold	Second Threshold
Scene-1	0.30	0.16
Scene-2	0.35	0.22
Scene-3	0.13	0.06
Scene-4	0.32	0.18
Scene-5	0.41	0.25
Scene-6	0.20	0.11
Scene-7	0.20	0.09

After detecting shadowy pixels, every detected local peak is analyzed according to shadows. In this step, position of shadows given as input to algorithm and the algorithm seeks shadowy pixels near the detected local peaks. If shadowy pixels are located near the local peak, the peak is approved as a treetop; otherwise the algorithm looks for another local peak in the focused area as the trees may be close to each other. Thus, the peak is also approved as treetop. If neither shadowy pixel nor local peak is detected in the focused area, that local peak is removed and is not labeled as a treetop.

In Figure 28, sample local peaks are denoted as numbers. The blue squares point out focus area. The focus area is determined according to shadow positions in the multispectral imagery. For instance, when the algorithm investigates the first local peak, it tracks the pixels in the square that is above the local peak. Then, it would detect shadowy pixels in the square and approves the local peak as treetop. On the other hand, when the algorithm passes the second local peak it will investigate the square above the peak and it cannot detect any shadowy pixel or local peak in the focused area. Thus, second local peak will not be claimed as treetop. Also, when the algorithm examines the third local peak, it cannot detect any shadowy pixel in the focused area, but it catch a local peak in the focused area and will approve the third local peak as treetop.

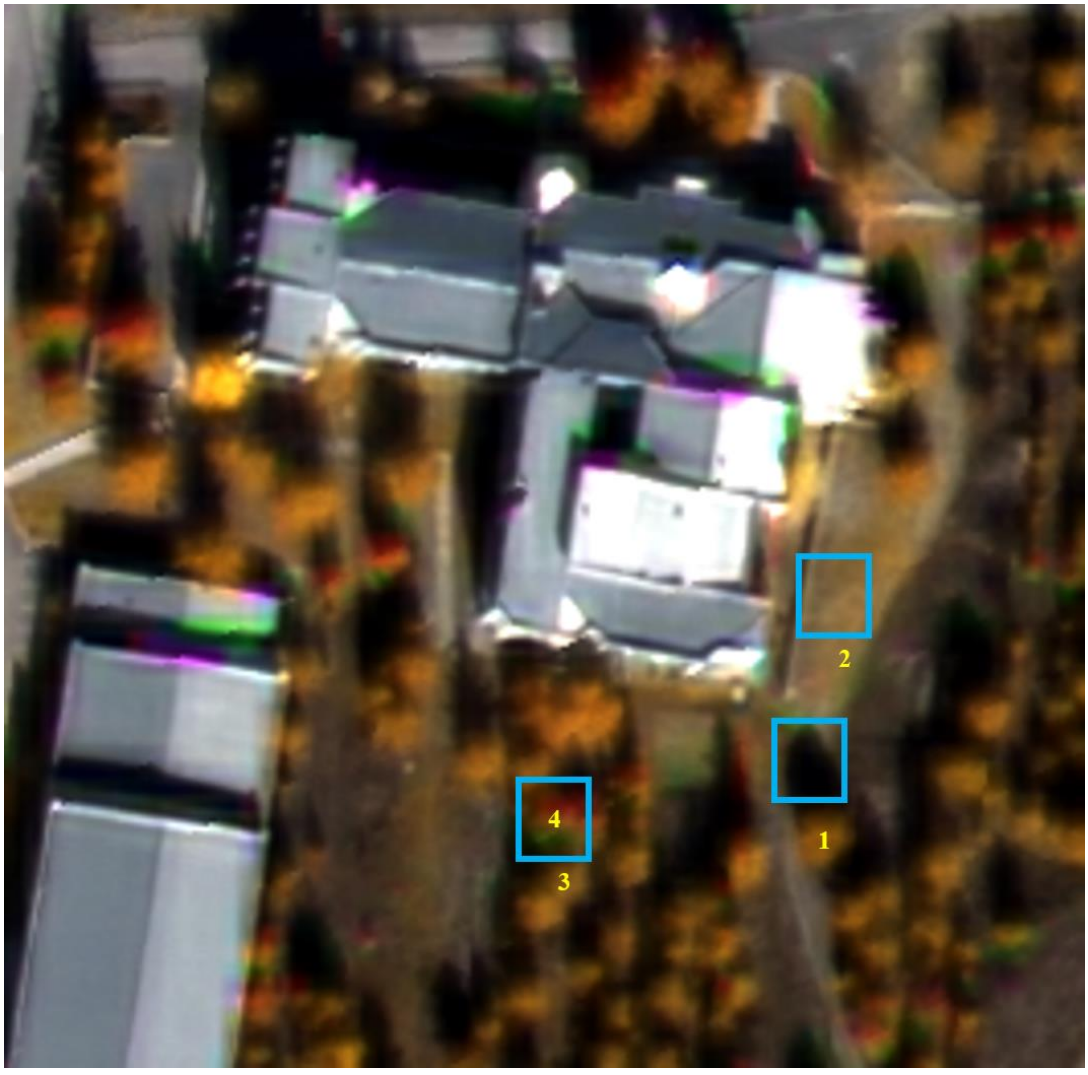

Figure 28: Sample of treetop validation based on shadows

CHAPTER 4

EXPERIMENTS

In this chapter, the experimental results of detection of pixels that belong to tree crown by vegetation indices and accuracy of detected treetops are demonstrated. The accuracy of vegetation indices and local maxima detection are calculated separately. The results of accuracy assessment of vegetation indices are demonstrated in Section 4.2. On the other hand, accuracy assessment of local maxima detection algorithm is demonstrated in Section 4.3. Lastly, the performance of treetop validation method is demonstrated in Section 4.4.

4.1 Measurement Metrics

Accuracy assessment for vegetation indices and local maxima detection can be done by various approaches. I used vegetation index accuracy for evaluating the accuracy of truly found pixels in the image. I calculated the accuracy as number of truly detected pixels divided by total number of pixel. The equation can be seen below:

$$Vegetation\ Index\ Accuracy\ = \frac{Number\ of\ Correctly\ Detected\ Pixels}{Number\ of\ All\ \text{Pixels}} \qquad (37)$$

I used precision, recall and F-Measure metrics to evaluate the performance of tree crown detection method. Before defining these metrics some terms that are related with them are introduced below:

True Positives (TP) is the number of correctly detected treetops.

False Positives (FP) is the number of incorrectly detected treetops. This metric includes the treetops that located more than one in tree crown.

False Negatives (FN) is the number of tree crowns that is not detected by the method.

Precision is the ratio of number of correctly detected tree crowns to number of all detected tree crowns.

$$Precision = \frac{TP}{TP + FP} \tag{38}$$

Recall is the ratio of number of correctly detected tree crowns to number of tree crowns in the ground truth.

$$Recall = \frac{TP}{TP + FN} \tag{39}$$

F-measure is defined as weighted harmonic mean of its precision and recall.

$$F_{\alpha} = \frac{(1 + \alpha)\ x\ Precision\ x\ Recall}{\alpha\ x\ Precision + Recall} \tag{40}$$

The α parameter is a non-negative scalar and in this study it is set to 0.5.

4.2 Experimental Accuracy Results of Vegetation Indices

Main goal of this section is determining the performance of detecting the pixels that contain tree crown correctly and discriminating them from other vegetated areas by using vegetation indices. Detailed information about this process is provided in Chapter 3. The analysis is made by comparing performance of different vegetation indices by calculating vegetation index accuracy due to extracted ground truth data.

I conducted the experiments by trying different threshold values for obtaining better results for each vegetation index. Firstly, I experienced performance of the vegetation indices developed by other researchers for vegetation detection. As mentioned before, I try to evaluate not the performance of detecting vegetated areas, but the performance of detecting only tree crown areas.

For the first experiment, thirteen vegetation indices are tested. In Table 13, accuracy of known vegetation indices can be seen.

Table 13: Accuracy of the known vegatation indices

Vegetation Index	Accuracy						
	Scene-1	Scene-2	Scene-3	Scene-4	Scene-5	Scene-6	Scene-7
NDVI1	87.17%	92.60%	93.49%	56.91%	86.62%	81.44%	92.07%
NIRRY	86.59%	91.43%	93.05%	56.20%	86.83%	81.51%	91.83%
normalizedRed	86.47%	88.60%	93.36%	56.54%	85.47%	81.45%	91.90%
normalizedNIR	83.85%	90.03%	91.17%	53.84%	87.15%	80.49%	91.50%
NDVI2	83.01%	84.78%	91.00%	55.80%	83.88%	80.36%	91.15%
ExGR	82.84%	83.71%	85.11%	52.84%	83.03%	75.27%	84.02%
ExG	82.53%	86.73%	82.61%	48.08%	81.89%	72.90%	84.02%
REY	82.03%	84.64%	90.12%	53.25%	84.00%	78.22%	89.63%
NYVI	81.93%	85.13%	89.87%	54.34%	83.29%	79.78%	89.70%
GNDVI	79.56%	85.92%	88.66%	47.18%	85.45%	78.55%	90.20%
ExR	68.75%	77.72%	82.61%	51.48%	82.37%	76.87%	84.97%
NDI	67.22%	77.72%	82.61%	50.99%	82.32%	77.03%	84.89%
ExB	67.15%	77.72%	82.61%	44.05%	80.93%	71.69%	84.02%

Figure 29 shows the chart of average accuracy of the known vegetation indices. The analysis of the Figure 29 showed the NDVI1 produced better results when compared to other vegetation indices. Also, the vegetation indices using NIR1 spectral band of WorldView multispectral imagery produced satisfying results. However, the vegetation indices utilizing only visible spectral bands (red, green, blue) produced poor results.

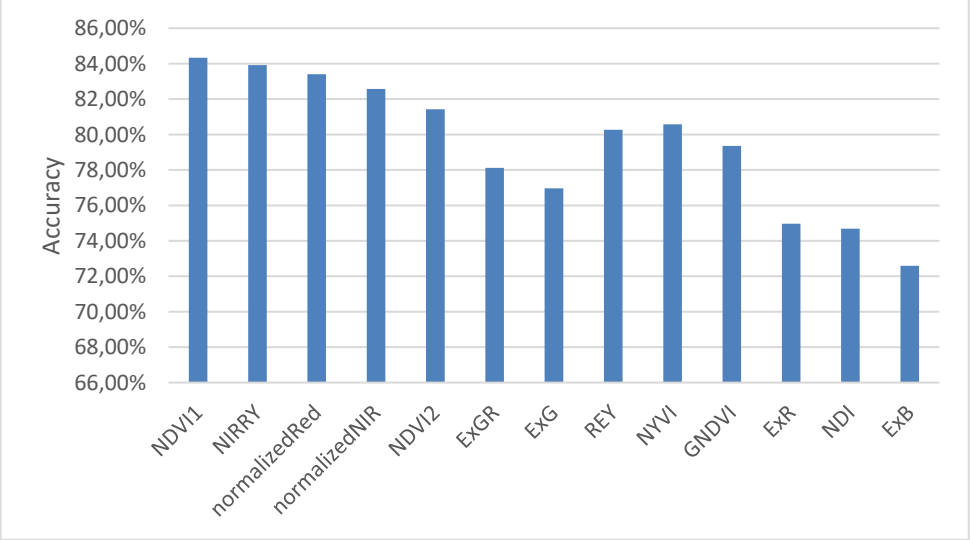

Figure 29: Average accuracy of the known vegatation indices for all scenes

Second experiments are conducted double combinations of these vegetation indices. In these experiments a pixel is marked as tree crown area when both of the vegetation indices votes that pixel as a tree crown. In Table 14, accuracy of double combination of vegetation indices can be seen. When I analyzed the accuracy results of double combinations of vegetation indices, some of them produces slightly better results than NDVI1. However, when I look at the Table 14 I cannot obtain significant upswing in accuracy.

Table 14: Accuracy of double combinations of vegetation indices

Vegetation Index		Accuracy						
		Scene-1	Scene-2	Scene-3	Scene-4	Scene-5	Scene-6	Scene-7
normalizedRed	NDVI1	87.24%	89.06%	93.85%	57.72%	86.45%	81.73%	92.09%
NIRRY	normalizedRed	87.05%	88.70%	93.58%	57.91%	86.23%	81.98%	91.99%
NIRRY	NDVI1	86.90%	91.66%	93.22%	57.05%	86.43%	81.76%	91.96%
normalizedRed	normalizedNIR	86.58%	88.19%	92.67%	56.73%	87.09%	81.64%	91.95%
normalizedNIR	NDVI1	86.48%	90.82%	92.18%	55.95%	87.26%	81.31%	91.90%
NIRRY	normalizedNIR	86.06%	90.49%	92.10%	55.20%	86.98%	81.28%	91.82%
GNDVI	normalizedRed	85.42%	86.14%	90.04%	52.27%	86.39%	80.91%	90.87%
GNDVI	NDVI1	85.31%	87.93%	89.53%	51.46%	86.54%	80.51%	90.78%
GNDVI	NIRRY	84.94%	87.74%	89.44%	50.76%	86.22%	80.37%	90.75%
ExGR	NDVI1	84.75%	86.45%	90.43%	57.48%	84.88%	77.45%	92.07%

Since accuracy results of double combinations of vegetation indices did not show significant improvements, I started to investigate different combinations of spectral bands for getting better results. Firstly, I tried to get better results by changing spectral bands of NDVI. Sample equation for proposed method is given below:

$$Vegetation\ Index = \frac{Band1 - Band2}{Band1 + Band2} \tag{41}$$

Table 15 indicates accuracy results of combinations of different spectral bands.

Table 15: Accuracy of different combinations of spectral bands

Vegetation Index	Accuracy						
	Scene-1	Scene-2	Scene-3	Scene-4	Scene-5	Scene-6	Scene-7
(NIR1 - Y) / (NIR1 + Y)	85.01%	89.32%	91.94%	55.16%	85.64%	80.88%	91.28%
(RE - R) / (RE + R)	83.70%	83.27%	92.32%	55.34%	84.42%	79.75%	91.46%
(RE - Y) / (RE + Y)	82.03%	84.64%	90.12%	53.25%	84.00%	78.22%	89.63%

Another experiment to find better vegetation index is conducted by calculating ratios of spectral bands as vegetation index. Sample equation for proposed method is given below:

$$Vegetation\ Index = \frac{Band1}{Band2} \tag{42}$$

Accuracy results for proposed method can be seen in Table 16. When I analyzed the results, ratio of NIR1 and red bands gave better results. However, their accuracy for discrimination of grass and tree crowns were not as high as NDVI1.

Table 16: Accuracy of simple ratio of spectral bands

Vegetation Index	Accuracy						
	Scene-1	Scene-2	Scene-3	Scene-4	Scene-5	Scene-6	Scene-7
NIR1 / R	87.2%	92.59%	93.53%	56.88%	86.62%	81.45%	92.07%
NIR1 / Y	85.00%	89.36%	91.95%	55.08%	85.66%	80.90%	91.27%
RE / R	83.73%	83.27%	92.35%	55.40%	84.48%	79.76%	91.47%

After that experiment I tried to get better results as normalizing a spectral band with sum of two spectral bands. Sample equation for proposed method is given below:

$$Vegetation\ Index = \frac{Band1}{Band1 + Band2} \tag{43}$$

Table 17 shows the top ten accuracy results of proposed method. Better results obtained by using red and NIR1 band of WorldView multispectral imagery as can be seen in Table 17. However, NDVI1 was still produce better results.

Table 17: Accuracy of ratio of double spectral bands vegetation indices

Vegetation Index	Accuracy						
	Scene-1	Scene-2	Scene-3	Scene-4	Scene-5	Scene-6	Scene-7
R / (R + NIR1)	87.15%	92.55%	93.51%	56.66%	86.62%	81.40%	92.05%
NIR1 / (R + NIR1)	87.12%	91.97%	93.47%	56.69%	86.62%	81.44%	92.05%
R / (Y + NIR1)	86.92%	90.36%	93.60%	56.94%	85.05%	80.70%	91.70%
R / (NIR1 + NIR2)	86.83%	90.62%	93.11%	56.85%	85.63%	81.03%	91.78%
R / (G + NIR1)	86.46%	89.57%	93.34%	57.01%	85.53%	81.35%	91.88%
R / (RE + NIR1)	86.35%	89.75%	93.47%	56.55%	86.06%	80.99%	92.04%
Y / (G + NIR1)	86.15%	87.29%	92.69%	56.67%	84.29%	80.85%	91.04%
NIR1 / (R + RE)	85.53%	87.90%	92.88%	56.59%	85.06%	79.55%	89.94%
Y / (RE + NIR1)	85.08%	89.63%	91.57%	54.67%	85.77%	80.32%	91.04%
Y / (NIR1 + NIR2)	85.06%	89.33%	91.66%	55.23%	85.25%	80.60%	90.76%

Sixth experiment conducted by normalizing a spectral band with sum of three spectral bands. Sample equation for proposed method is given below:

$$Vegetation\ Index = \frac{Band1}{Band1 + Band2 + Band3} \tag{44}$$

Table 18 shows the top ten accuracy results of proposed method. Better results obtained by using yellow, red and NIR1 band of WorldView multispectral imagery as can be seen in Table 18. However, NDVI1 still produced better results.

Table 18: Accuracy of ratio of triple spectral bands vegetation indices

Vegetation Index	Accuracy						
	Scene-1	Scene-2	Scene-3	Scene-4	Scene-5	Scene-6	Scene-7
R / (R + NIR1 + NIR2)	86.77%	90.51%	93.04%	56.92%	85.55%	81.02%	92.05%
R / (Y + R + NIR1)	86.68%	90.47%	93.41%	56.55%	84.89%	80.66%	92.05%
R / (G + NIR1 + NIR2)	86.65%	89.17%	93.50%	57.48%	85.27%	81.13%	91.70%
NIR1 / (Y + R + NIR1)	86.59%	91.16%	92.96%	56.29%	86.82%	81.51%	91.78%
Y / (B + RE + NIR1)	86.39%	87.60%	93.44%	57.30%	84.87%	81.09%	91.88%
Y / (G + RE + NIR1)	86.36%	89.13%	92.39%	56.38%	84.80%	80.61%	92.04%
R / (Y + NIR1 + NIR2)	86.29%	88.98%	93.19%	57.12%	84.83%	80.75%	91.04%
R / (R + RE + NIR1)	86.28%	89.74%	93.37%	56.44%	86.02%	81.00%	89.94%
Y / (G + NIR1 + NIR2)	86.27%	88.79%	92.55%	56.71%	84.54%	80.71%	91.04%
Y / (B + NIR1 + NIR2)	86.17%	87.03%	93.21%	57.54%	84.47%	80.97%	90.76%

Finally, some self-developed vegetation indices are tested for better detection accuracy. The proposed vegetation indices and their formulations are described in the Section 3.3. Table 19 indicates accuracy results of proposed vegetation indices.

Table 19: Accuracy of self-developed vegetation indices

Vegetation Index	Formula	Accuracy						
		Scene-1	Scene-2	Scene-3	Scene-4	Scene-5	Scene-6	Scene-7
index1	(2 * nir) - re - r	85.5%	87.92%	92.85%	56.61%	85.06%	79.54%	89.93%
index2	(2.5 * nir) - re - r	85.54%	87.9%	92.86%	56.47%	85.01%	79.54%	89.94%
index3	(1.4 * re) - nir	78.09%	81.51%	89.53%	54.48%	81.45%	73.87%	87.08%
index4	(1.74 * r) - nir	87.19%	92.61%	93.50%	56.83%	86.57%	81.45%	92.02%
index5	nir - r	86.98%	92.12%	93.41%	56.79%	86.57%	81.26%	91.91%
index6	(2 * nir) - (1.4 * r)	86.81%	91.43%	93.31%	56.91%	86.41%	81.01%	91.67%
index7	nir – re	80.16%	82.53%	90.64%	55.40%	82.09%	75.32%	87.81%
index8	(((2 * NIR1 + NIR2) / 3) - R) / (((2 * NIR1 + NIR2) / 3) + R)	87.06%	91.32%	93.22%	56.75%	85.71%	80.89%	91.73%

4.3 Experimental Accuracy Results of Local Maxima Detection

The second stage of the proposed method is detecting local maxima as the treetop in the preprocessed image. In this step, each detected treetop actually refers to a tree crown. For evaluating the local maxima detection method different window sizes, different sigma values for Gaussian filter and different spectral bands of satellite imagery are examined. Since NDVI1 produced relatively better results for detecting tree crown pixels, the experiments were made on the image that is masked by NDVI1 threshold. For evaluating the performance of the method, precision, recall and F-Measure metrics are calculated. If local maxima detection algorithm detects a pixel within a tree crown, that hit is taken as TP.

First experiment is conducted for evincing the best spectral band for local maxima detection algorithm. Appropriate window size and sigma value is selected for each scene in this step. Since vegetation employs red and near infrared bands for photosynthesis, only red, red edge, NIR1 and NIR2 bands of multispectral imagery are tested. In addition these bands green band is also tested. Table 20 indicates performance metrics of desired experiment. The accuracy results show that NIR1 band of the WorldView imagery is the best spectral band for local maxima detection in tree crown areas.

Table 20: Performace metrics of different spectral bands

Scene	Spectral Band	F-Measure	Precision	Recall
1	NIR-1	89.16%	91.93%	84.09%
	Red Edge	79.20%	81.48%	75.00%
	NIR-2	77.48%	81.17%	71.02%
	Green	76.20%	70.67%	90.34%
	Red	72.48%	68.57%	81.82%
2	NIR-1	92.70%	96.51%	85.92%
	Red Edge	84.98%	88.80%	78.24%
	NIR-2	83.32%	86.12%	78.24%
	Green	83.60%	83.01%	84.83%
	Red	77.72%	76.76%	79.71%
3	NIR-1	89.60%	89.90%	89.00%
	Red Edge	85.57%	85.86%	85.00%
	NIR-2	83.33%	82.52%	85.00%
	Green	72.93%	67.18%	88.00%
	Red	67.04%	62.02%	80.00%
4	NIR-1	51.74%	41.86%	98.09%
	Red Edge	34.55%	26.54%	87.02%
	NIR-2	39.13%	31.34%	77.86%
	Green	22.90%	16.85%	81.30%
	Red	26.80%	20.29%	74.81%
5	NIR-1	91.90%	95.24%	85.89%
	Red Edge	80.79%	81.65%	79.14%
	NIR-2	80.39%	83.11%	75.46%
	Green	83.09%	84.52%	80.37%
	Red	82.45%	83.87%	79.75%
6	NIR-1	66.67%	61.73%	79.37%
	Red Edge	58.67%	54.32%	69.84%
	NIR-2	62.11%	57.32%	74.60%
	Green	47.55%	41.58%	66.67%
	Red	43.64%	37.74%	63.49%
7	NIR-1	77.16%	76.57%	78.36%
	Red Edge	67.11%	66.48%	68.42%
	NIR-2	70.73%	71.01%	70.18%
	Green	59.47%	56.85%	65.50%
	Red	55.71%	52.40%	63.74%

Secondly, NIR1 band and appropriate sigma value for each scene are used in order to trace effects of different window sizes for local maxima detection algorithm. The accuracy results for different window sizes are presented in Table 21.

Table 21: Performace metrics of different window sizes

Scene	Window Size	F-Measure	Precision	Recall
1	3x3	86.50%	84.95%	89.77%
	5x5	89.16%	91.93%	84.09%
	7x7	83.11%	91.79%	69.89%
2	3x3	92.70%	96.51%	85.92%
	5x5	92.14%	97.63%	82.82%
	7x7	90.69%	97.53%	79.52%
3	3x3	85.45%	81.74%	94.00%
	5x5	89.60%	89.90%	89.00%
	7x7	85.71%	88.89%	80.00%
4	3x3	51.74%	41.86%	98.09%
	5x5	52.40%	45.03%	77.86%
	7x7	50.97%	47.31%	60.31%
5	9x9	91.06%	91.82%	89.57%
	11x11	91.90%	95.24%	85.89%
	13x13	90.48%	95.68%	81.60%
6	15x15	64.20%	57.78%	82.54%
	17x17	66.67%	61.73%	79.37%
	19x19	64.19%	60.53%	73.02%
7	15x15	75.41%	72.77%	81.29%
	17x17	77.16%	76.57%	78.36%
	19x19	76.06%	77.64%	73.10%

Finally, different sigma values are tested for better detection accuracy and tracing effects on the proposed method. NIR1 band and relevant window is used for this experiment. The accuracy results for blurring effects can be seen in Table 22.

Table 22: Performace metrics of different sigma values

Scene	Sigma Value	F-Measure	Precision	Recall
1	0.3	87.65%	89.22%	84.66%
	0.5	89.16%	91.93%	84.09%
	0.7	87.76%	92.16%	80.11%
	1.5	83.63%	91.30%	71.59%
2	0.3	92.23%	95.19%	86.84%
	0.7	92.70%	96.51%	85.92%
	1.5	91.82%	96.23%	84.10%
3	0.3	85.58%	83.96%	89.00%
	0.7	88.41%	88.12%	89.00%
	0.9	89.60%	89.90%	89.00%
	1.5	87.58%	87.88%	87.00%
4	0.3	45.25%	35.64%	98.09%
	0.7	51.74%	41.86%	98.09%
	1.5	51.62%	42.67%	88.93%
5	0.3	88.54%	90.26%	85.28%
	0.7	91.90%	95.24%	85.89%
	1.5	87.59%	93.38%	77.91%
6	1.5	63.64%	58.33%	77.78%
	2.0	66.67%	61.73%	79.37%
	2.5	62.79%	59.21%	71.43%
7	1.5	74.59%	72.11%	80.12%
	2.0	77.16%	76.57%	78.36%
	2.5	75.15%	75.90%	73.68%

Finally, although the values for parameters of local maxima detection are directly related with tree crown sizes on the multispectral imagery, the values listed in the Table 23 is recommended for study area according to experimental results for local maxima detection.

Table 23: Recommended values for parameters of local maxima detection

Imagery	Spectral Band	Window Size	Sigma Value	NDVI Threshold
WorldView-2	NIR1	5x5	0.7	0.23
WorldView-3	NIR1	15x15	2.0	0.40

4.4 Experimental Accuracy Results of Treetop Validation

In the last step of tree detection process, I attempted to remove false detections by using shadows on the scenes. Further explanation about this method can be seen in Section 3.5. The accuracy results of before applying this method and after applying this method for each scene is listed in Table 24.

Table 24: Performance metrics of shadow based treetop validation

Scene	Before/After Treetop Validation	F-Measure	Difference	Precision	Difference	Recall	Difference
1	Before	89.16%	3.00%	91.93%	6.05%	84.09%	-1.70%
	After	92.16%		97.97%		82.39%	
2	Before	92.55%	1.11%	96.49%	2.44%	85.56%	-0.91%
	After	93.66%		98.93%		84.64%	
3	Before	89.38%	4.09%	90.63%	7.10%	87.00%	-1.00%
	After	93.48%		97.73%		86.00%	
4	Before	51.74%	42.76%	41.86%	51.82%	98.09%	-1.91%
	After	94.50%		93.68%		96.18%	
5	Before	91.90%	0.40%	95.24%	0.65%	85.89%	0.00%
	After	92.31%		95.89%		85.89%	
6	Before	66.67%	20.08%	61.73%	32.39%	79.37%	-4.37%
	After	86.75%		94.12%		75.00%	
7	Before	77.16%	0.90%	76.57%	1.34%	78.36%	0.00%
	After	78.06%		77.91%		78.36%	

Comparison of F-Measures for each scene can be seen in Figure 30. It can be inferred from Figure 30 the validation process of detected local peaks leaded to an increase of F-Measure.

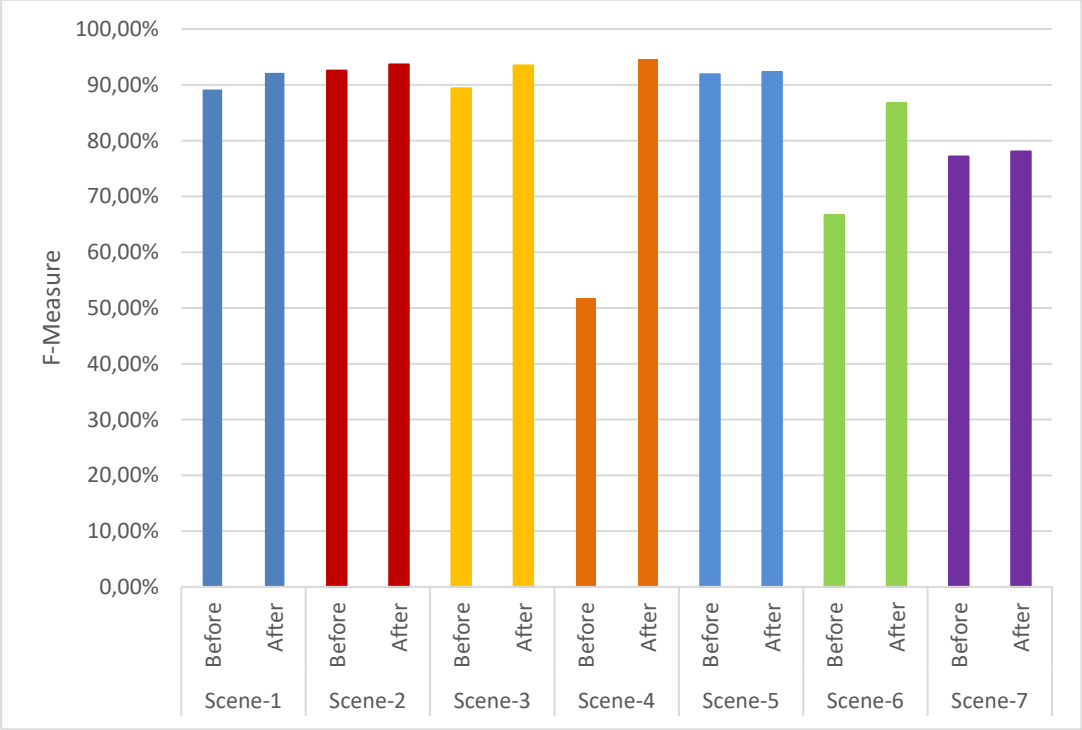

Figure 30: Comparative F-Measures of the each scene

Sample precision recall curve for Scene-2 is depicted in Figure 31. This curve shows precision and recall values for different NDVI threshold. The larger area under the curve indicates a better performance. Thus, when score of the NDVI, treetop detection using local maxima detection algorithm and treetop validation by shadows is analyzed, it can be clearly seen from the Figure 31 that each step of the proposed method helps to improve accuracy. In addition, better accuracy results are achieved by applying NDVI with threshold value of 0.19. Moreover, lower threshold value causes higher recall and lower precision, whereas higher threshold value produces higher precision but reduces recall.

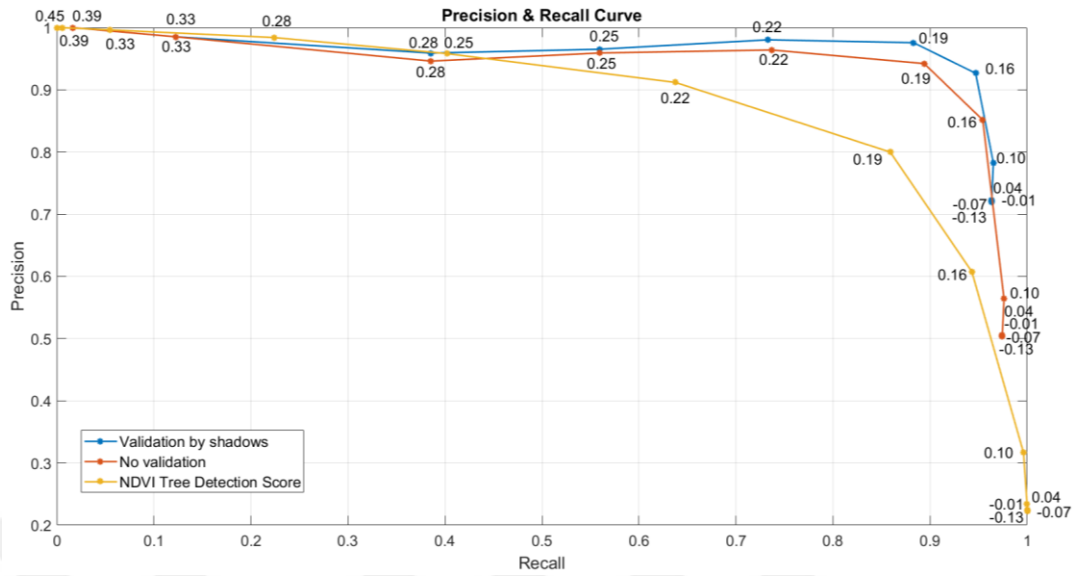

Figure 31: Precision Recall Curve

Results of proposed method is compared with local maxima detection method proposed by Daliakopoulos et al. [1]. The comparative results is listed in Table 25. It is seen that the proposed method outperforms [1] for all scenes and all measures.

Table 25: Comparison of tree crown detection methods

Scene	Proposed Method			The Method of Daliakopoulos et al. [1]		
	F-Measure	Precision	Recall	F-Measure	Precision	Recall
1	92.16%	97.97%	82.39%	80.94%	80.79%	81.25%
2	93.66%	98.93%	85.56%	90.83%	95.94%	82.08%
3	93.48%	97.73%	86.00%	82.65%	83.51%	81.00%
4	94.50%	93.68%	96.18%	50.30%	45.60%	63.36%
5	92.31%	95.89%	85.89%	79.01%	77.78%	81.60%
6	86.75%	94.12%	75.00%	49.14%	45.24%	59.38%
7	78.06%	77.91%	78.36%	58.73%	56.06%	64.91%

The final detected trees, undetected trees, the peaks that are incorrectly detected as treetops and removed local peaks by treetop validation process for each scene are represented in Figure 32-38. In these figures, rightly detected treetops are shown by green plus sign, the undetected treetops are marked as red multiplication sign, the incorrectly detected treetops are pointed with yellow circles, and the removed local peaks by shadow based validation are marked as blue circles. All of the scenes in the Figure 32 - Figure 38 represented as both true and false color image.

(a)

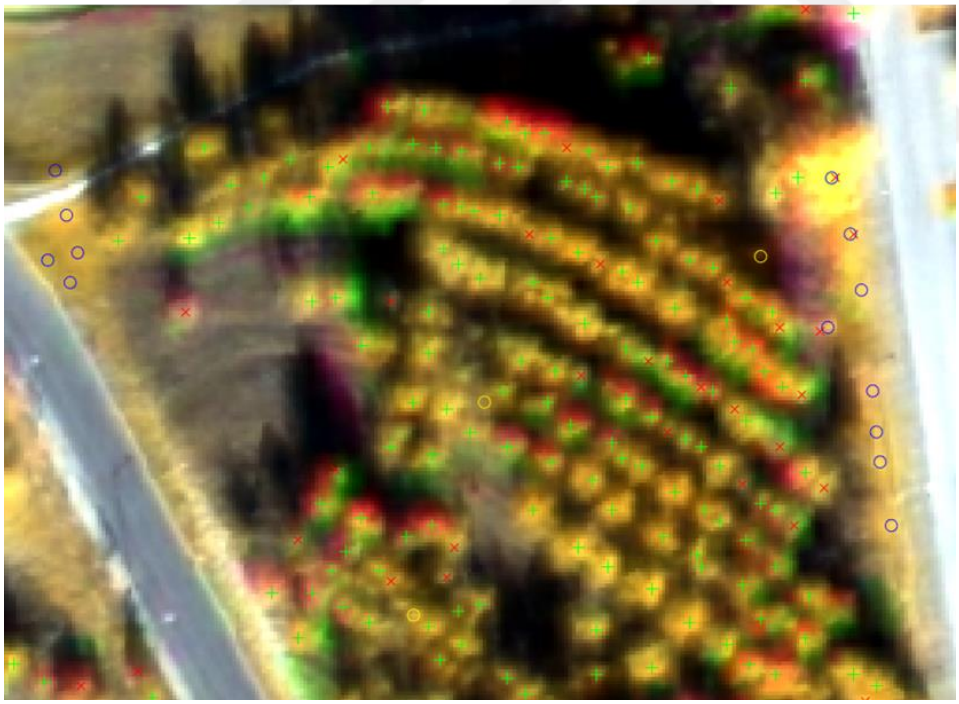

(b)

Figure 32: (a) Results of Scene-1 RGB image (b) false color image

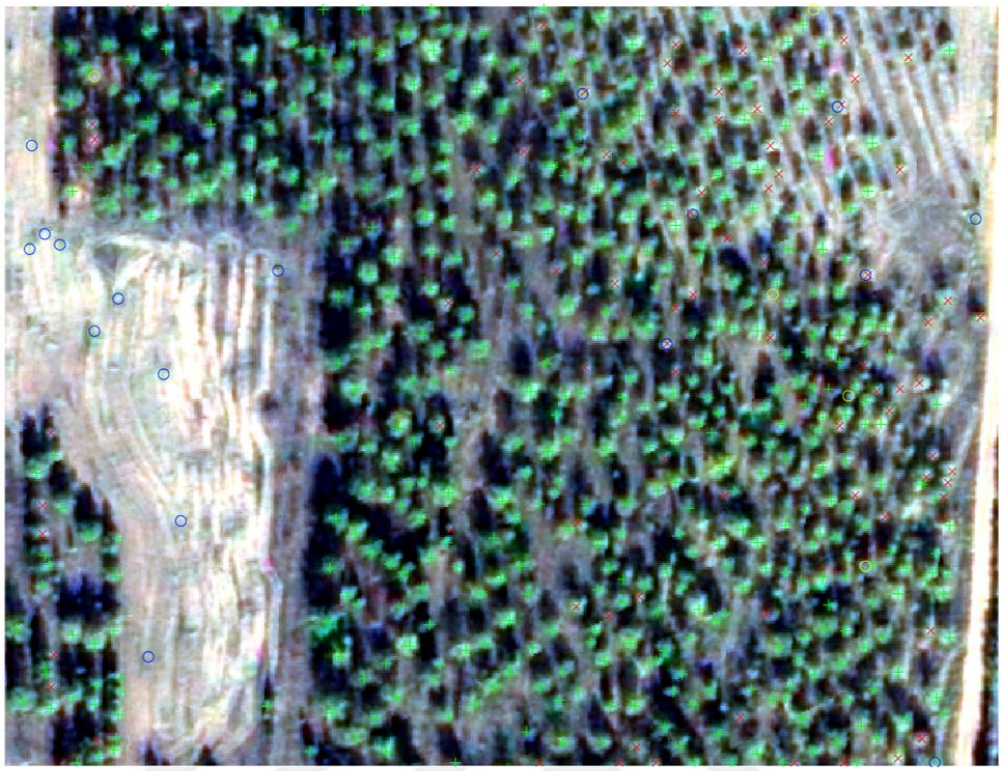

(a)

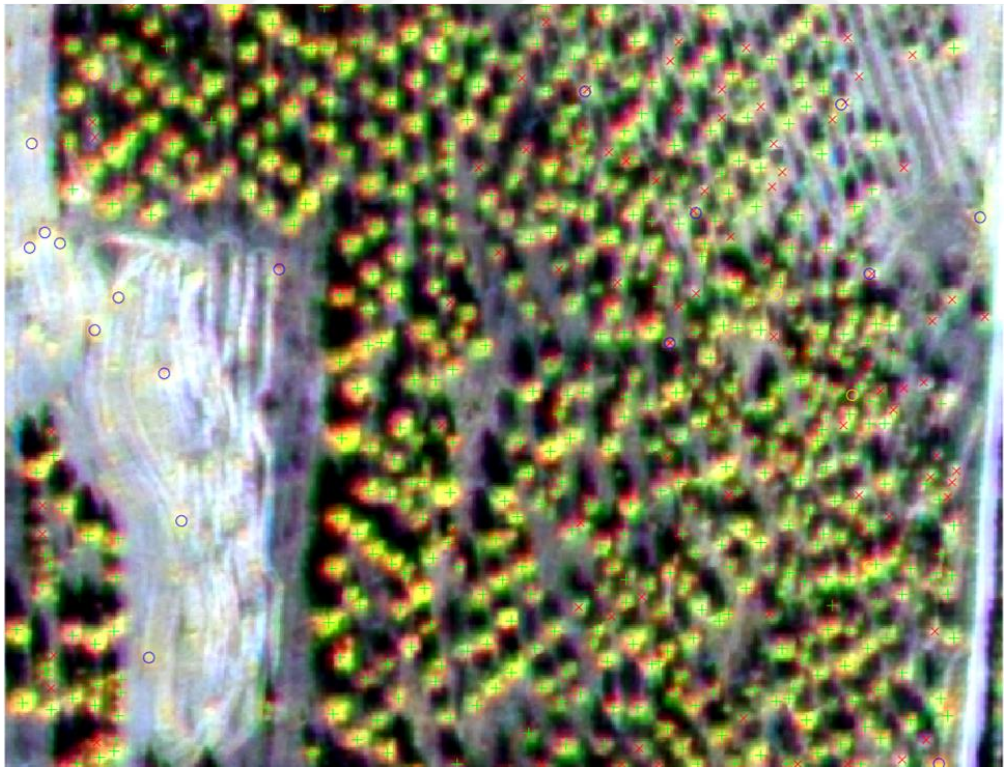

(b)

Figure 33: (a) Results of Scene-2 RGB image (b) false color image

(a)

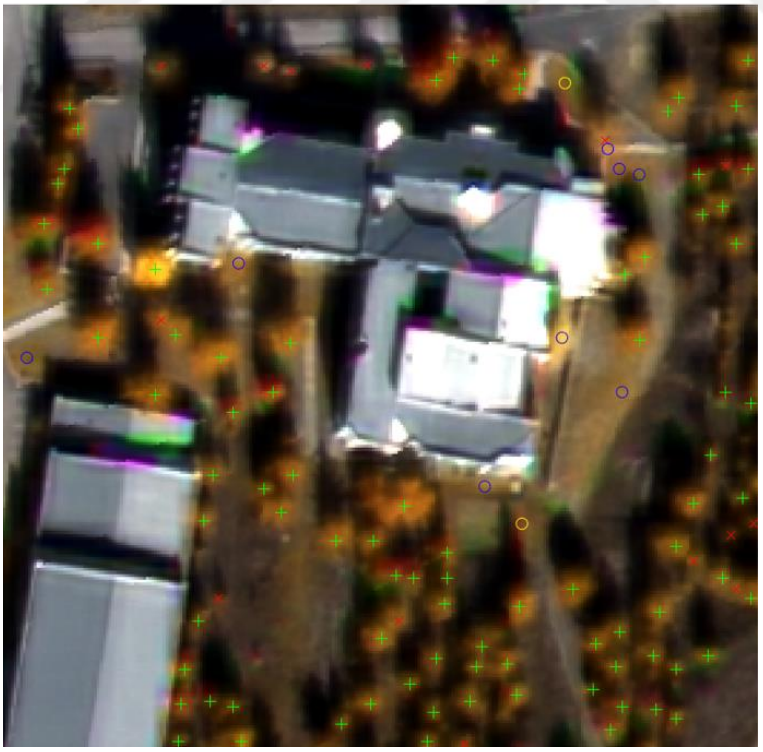

(b)

Figure 34: (a) Results of Scene-3 RGB image (b) false color image

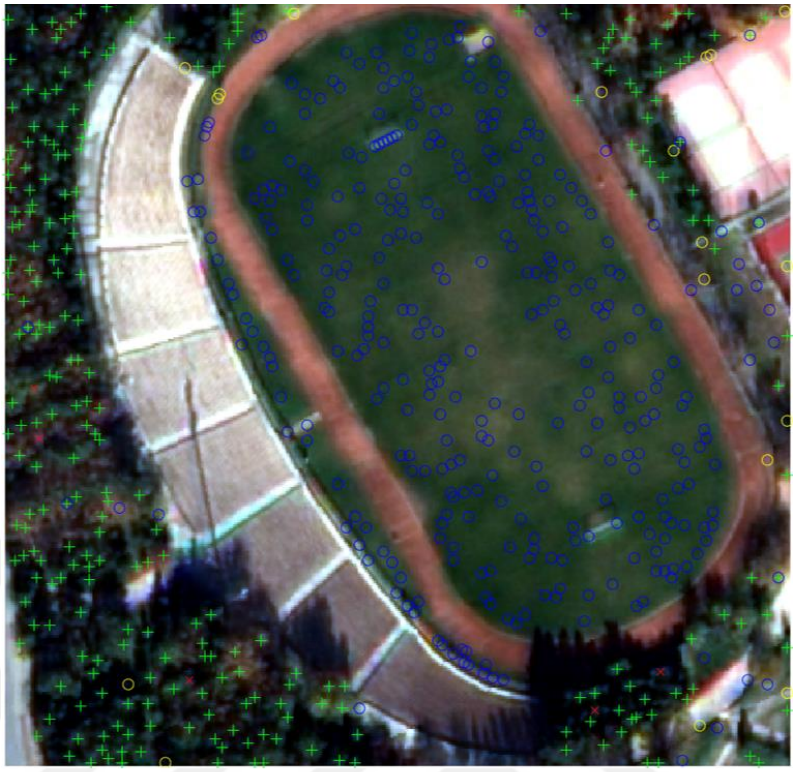

(a)

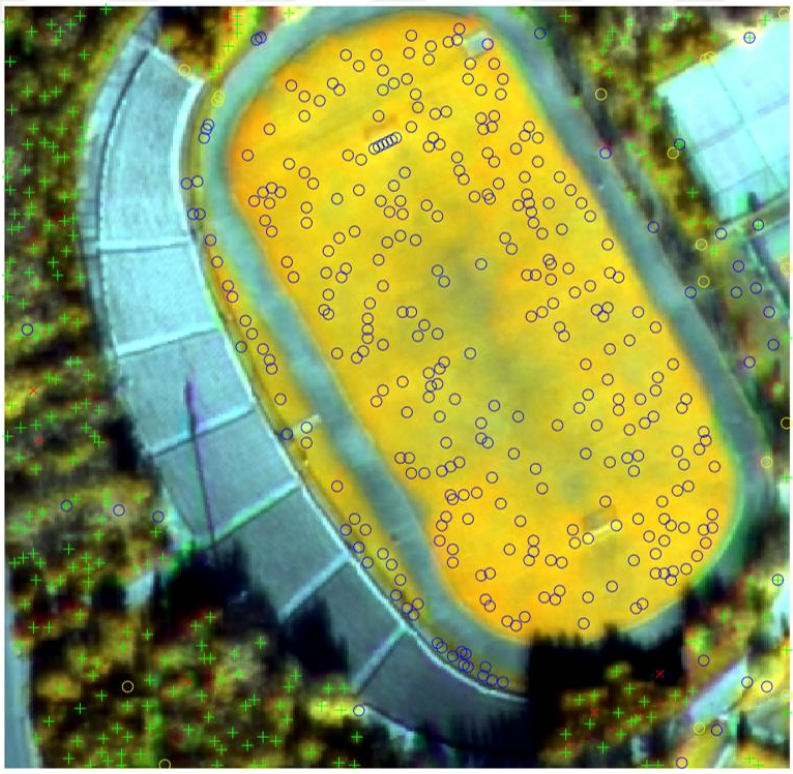

(b)

Figure 35: (a) Results of Scene-4 RGB image (b) false color image

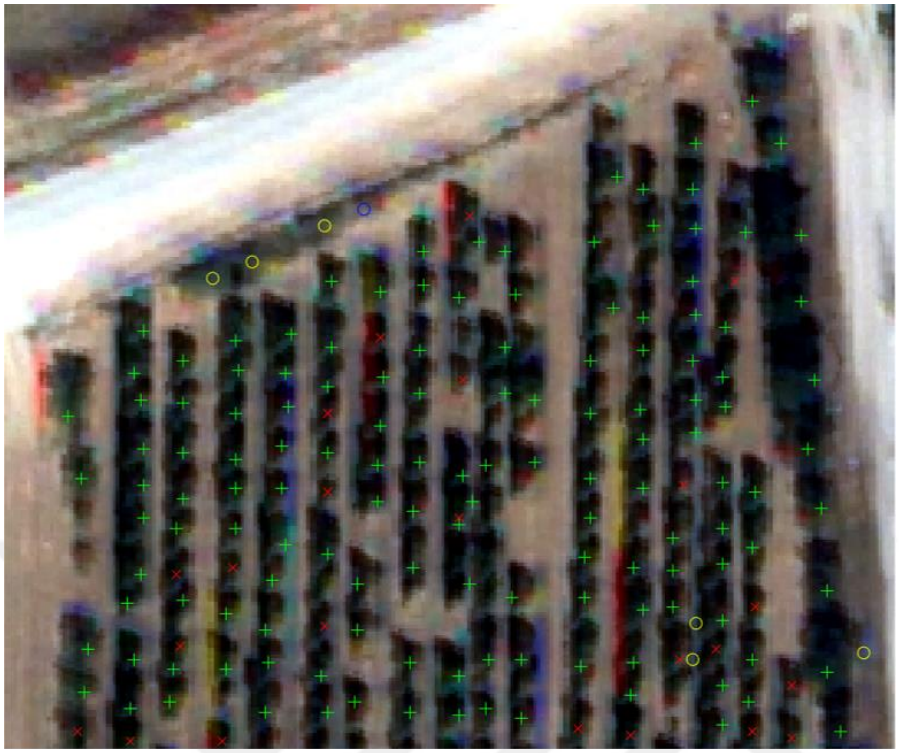

(a)

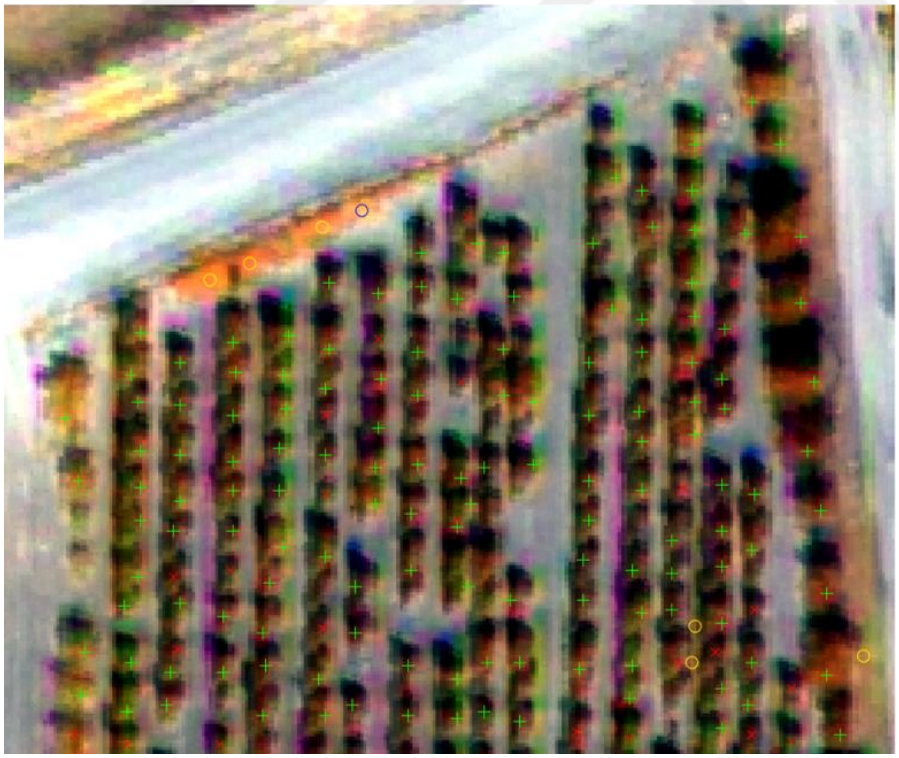

(b)

Figure 36: (a) Results of Scene-5 RGB image (b) false color image

(a)

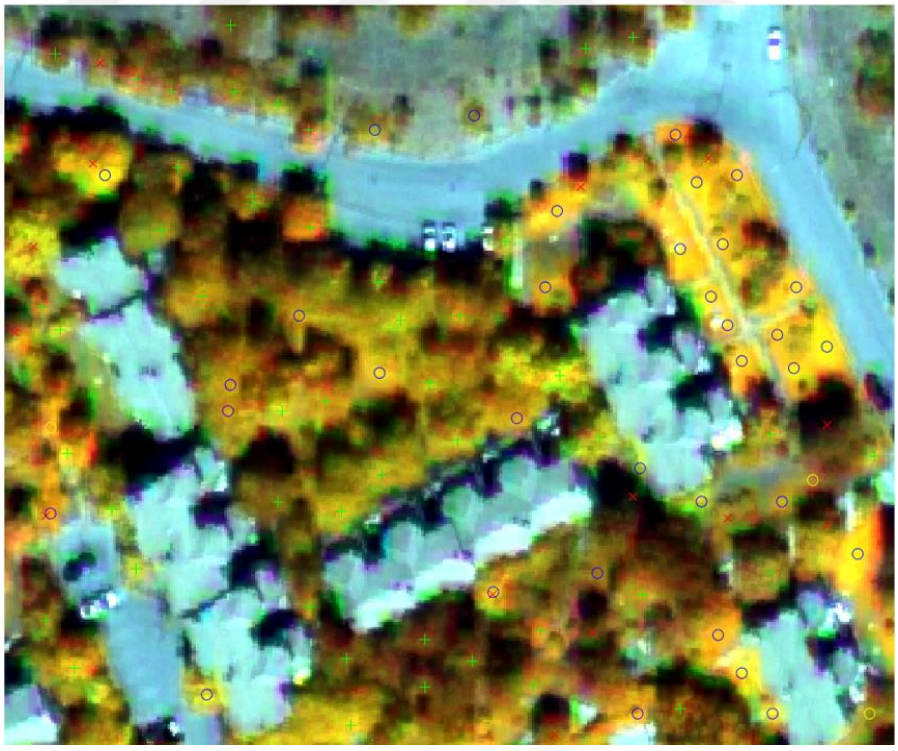

(b)

Figure 37: (a) Results of Scene-6 RGB image (b) false color image

(a)

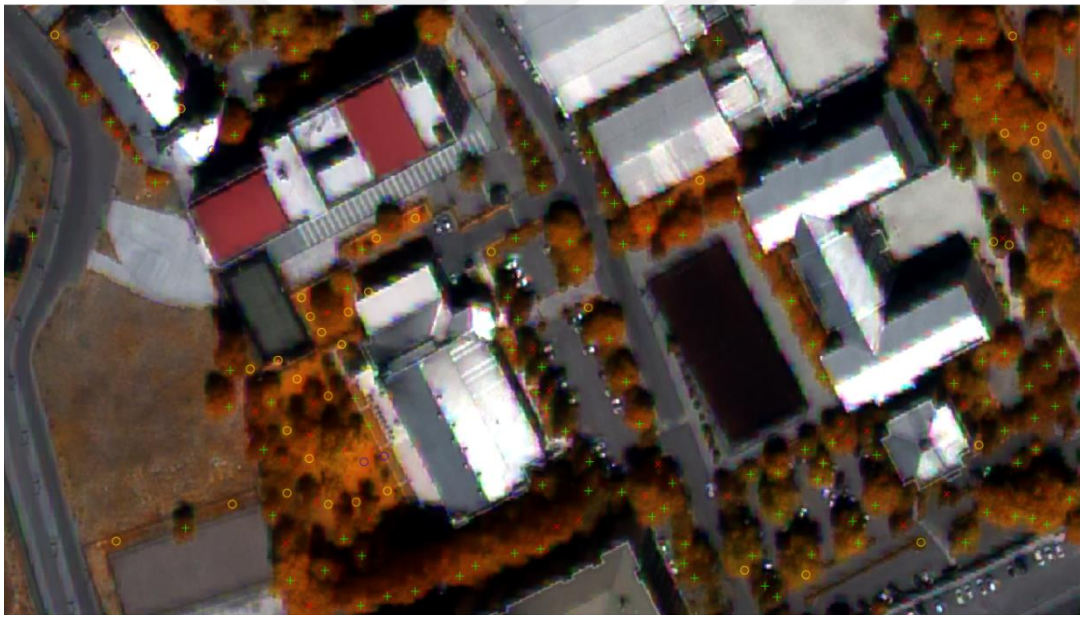

(b)

Figure 38: (a) Results of Scene-7 RGB image (b) false color image

CHAPTER 5

CONCLUSION

5.1 Summary

In this study, thirteen different vegetation indices and their pairwise combinations are analyzed for detecting trees on very high resolution multispectral imagery. In addition to these vegetation indices, different combinations of spectral bands and transformation of some vegetation indices are investigated for better performance. Also, the effects of Gaussian filter, different window sizes and different spectral bands on local maxima detection algorithm analyzed and better values of these variables are investigated for treetop detection. Moreover, the detected local peaks are validated according to existence of shadows in their neighborhood. Seven different areas are extracted from multispectral imagery for aforementioned experiments. First four scenes were acquired by WorldView-2 sensor. The other three scenes were acquired by WorldView-3 sensor. HCS pan-sharpening method were applied to all scenes to increase spatial resolution of multispectral imagery.

Vegetation indices and their different variations are analyzed in order to evaluate performance of detecting only tree crowns instead of whole vegetated areas. Accuracy of different vegetation indices produced similar results for the tested scenes. The vegetation indices that occupy only visible spectral bands gave poor results when compared with the vegetation indices that occupy near infrared bands. NDVI1 which is commonly used vegetation index by other researchers produced satisfying results, but combination of NDVI1 and with different vegetation indices produced slightly better results. For instance, while using combination of NDVI1 and normalizedRed produced increased accuracy for Scenes 1, 3, and 7; using combination of NDVI1 and normalizedNIR produced limited increment on accuracy for Scene-5.

On the other hand, replacing the spectral bands of NDVI1 with different spectral bands could not present any melioration for detecting tree crown pixels. Another analyzed vegetation index was simple ratio of two different spectral bands. When I analyzed the result of this type of vegetation index, ratio of NIR1 and red produced slightly better results than NDVI1. However, it was not significant. Our research continued with tracking improved accuracy with vegetation indices that normalize a spectral band with sum of two or three spectral bands. However, none of the experimented vegetation indices improved performance when compared to NDVI1.

Moreover, some vegetation indices developed in this research by conducting some equations utilizing different spectral bands. Among this self-developed vegetation indices, so-called Index4 produced slightly better result than NDVI1 for all scenes except Scene-4 and Scene-7. However, these results could not meet our expectations for removing grassy areas from vegetated regions. Furthermore, when I analyzed the overall results for usage of new multispectral bands of WorldView-2 and WorldView-3 multispectral imagery in vegetation indices did not produce better results. On the other hand, since Scene-4 and Scene-6 includes more grassy regions compared to other scenes, vegetation indices represented poorer performance for these scenes.

Local maxima detection method was the second stage of tree crown detection process. The best results for this method were obtained by using NIR1 band. Additional NIR2 band of WorldView-2 and WorldView-3 multispectral imagery did not produce better results for treetop detection as most of tree crowns analyzed in this study have higher reflectance in the NIR1 bands. This can be seen on the figures showing the spectral plot of sample trees between Figure 7 - 19.

Furthermore, experiments for different window sizes for local maxima detection are conducted. While smaller window sizes produced better performance for the scenes cropped from WorldView-2 imagery, higher window sizes improved the accuracy for the scenes selected from WorldView-3 imagery. The main reason of this issue is the different spatial resolution of WorldView-2 and WorldView-3 imagery. Also, since the tree crowns have higher diameter size on Scenes-6 and 7, higher window size produced better performance. Hence, window size should be selected with spatial resolution and crown sizes on the image. Consequently, while selection of higher window sizes caused underestimation of the treetops, lower window sizes caused overestimation of treetops.

In addition to analysis on different window sizes, different blurring ratios for Gaussian filter are practiced. When the results of experiments are investigated, higher sigma values produced higher accuracy for Scene-6 and 7. On the contrary, lower sigma values produced better performance for the other scenes. Experiments showed that optimum sigma value is affected by the size of the tree crown. Since larger tree crowns could include more than one local peak, optimum sigma value is set to be large so that clusters of peaks are grouped together. Too high resulted in degradation of detecting treetops, whereas frequent tree crowns caused poorer accuracy results due to overlaps of tree crowns.

Furthermore, the local maxima detection algorithm produced better accuracy in the scenes including mainly coniferous trees (Scene-1 to 5). The conical shape of coniferous trees mostly gives only one treetop in the tree crown, whereas deciduous trees can have more than one treetop in the tree crown. Consequently, one reason for poorer performance in Scene-6 and 7 is that these scenes include more coniferous trees than the other ones.

In final stage of proposed method, since I could not eliminate grassy areas completely using vegetation indices, I decided to validate detected local peaks by tracing shadows around the detected local peaks. I utilized a shadow detection method to identify shadows on the study area. Experiments showed that this method can cause considerable improvement on precision. As a result of improved precision, F-Measure was increased. If a scene contains wide grassy areas, F-Measure increases more. For instance, analysis on Scene-4 showed that this validation causes almost 43% improvements on F-Measure. Thus, this method is suitable for scenes that contain wide grassy areas.

The results of conducted experiments can be summarized as listed below:

- Utilizing vegetation indices is not efficient way for discriminating tree crowns and other vegetated areas on the multispectral imagery.
- Usage of new spectral bands of WorldView-2 and WorldView-3 multispectral imagery in vegetation indices does not provide an improvement for selection of tree crowns.
- Local maxima detection algorithm is suitable for the scenes which include almost same size of tree crowns.
- Utilizing local maxima algorithm for the scenes that contains cone-shaped coniferous trees are more practical owing to shape of the crown.
- Designation of window size and sigma value appropriately would produce better performance.
- Removal of incorrectly detected treetops by using shadows can ensue significant improvement on treetop detection process on grassy areas.

Although proposed method produced satisfying performance in the conducted experiments, some limitations of this method can be listed as below:

- Since the experiments were conducted on the multispectral images that are acquired in July and November, the proposed method may produce different performance on the images acquired in spring due to higher spectral reflectance of grass in near infrared spectra.
- Since the study area of this study includes similar vegetation cover, the proposed method could produce different performance for different vegetation cover.

Finally, I compared the tree crown detection results with literature. Since there is no prepared datasets and ground truth, researchers were used different multispectral images from different areas. Also, most of them extracted their ground truth data by themselves. I acquired reasonably 92.71% for detecting tree crowns in forested area, 88.20% for detecting tree crowns in urban area. Srestasathiern and Rakwatin utilized NDI before local maxima process for detecting oil palm trees and their F-measure values ranging from 0.897 to 0.981 for different scenes of WorldView-2 imagery. Since the oil palm trees in their scenes do not overlapped and show regular form, their algorithm produced very accurate results [13]. Daliakoloulos et al. combined red band

and NDVI thresholds with Laplacian of Gaussian blob detection. The error rate shows their algorithm extracted 86.7% of the actual trees [1]. Gomes and Maillard attempted tree crown identification in a tropical environment by using NDVI and region growing method. They reported an accuracy over 80% [45]. Mohour et al. utilized grey-level blob detection and scale-space blob detection for detecting trees and they acquired 81.6% and 90% of the trees for two different areas [46].

5.2 Future Work

I employed the tree crown detection method on seven remotely sensed imageries. Although the results that are obtained in this study are promising, experiments with different scenes should also be performed to support these results. The performance under different location, time and weather conditions should be determined. On the other hand, extracting ground truth data accurately is very important for accuracy calculation. For this reason, publishing public multispectral datasets and ground truth will make measuring and comparing proposed methods easier.

Thresholds for vegetation indices can be determined by automated processes. On the other hand, further improvements for using local maxima algorithm with adaptable window size are needed.

Finally, since usage of shadows for validating detected treetops is a novel method, further research should be conducted on different datasets. Also, different shadow detection algorithms and shape based shadow-tree pairing can be studied in further studies.

REFERENCES

[1] I. N. Daliakopoulos, E. G. Grillakis, A. G. Koutroulis, and I. K. Tsanis, "Tree crown detection on multispectral VHR satellite imagery," *Photogramm. Eng. Remote Sensing*, vol. 75, no. 10, pp. 1201–1211, 2009.

[2] "What is remote sensing?" [Online]. Available: https://crisp.nus.edu.sg/~research/tutorial/intro.htm.

[3] K. C. Sahu, *Textbook of remote sensing and geographical information systems*. Atlantic Publishers & Dist, 2007.

[4] "Remote Sensors." [Online]. Available: https://earthdata.nasa.gov/user-resources/remote-sensors.

[5] S. Rajendran, *Hyperspectral remote sensing and spectral signature applications*, no. December. New India Publishing, 2009.

[6] M. Kubo, S. Nishikawa, E. Yamamoto, and K. I. Muramoto, "Identification of individual tree crowns from satellite image and image-to-map rectification," *Int. Geosci. Remote Sens. Symp.*, pp. 1905–1908, 2007.

[7] C. Padwick, P. Scientist, M. Deskevich, F. Pacifici, and S. Smallwood, "WorldView-2 pan-sharpening," *Asprs 2010*, vol. 48, no. 1, pp. 26–30, 2010.

[8] M. Immitzer, C. Atzberger, and T. Koukal, "Tree species classification with random forest using very high spatial resolution 8-band WorldView-2 satellite data," *Remote Sens.*, vol. 4, no. 9, pp. 2661–2693, 2012.

[9] M. Karlson, H. Reese, and M. Ostwald, "Tree crown mapping in managed woodlands (Parklands) of semi-arid West Africa using WorldView-2 imagery and geographic object based image analysis," *Sensors (Switzerland)*, vol. 14, no. 12, pp. 22643–22669, 2014.

[10] A. Huete, K. Didan, T. Miura, E. P. Rodriguez, X. Gao, and L. G. Ferreira, "Overview of the radiometric and biophysical performance of the MODIS vegetation indices," vol. 83, pp. 195–213, 2002.

[11] D. M. Woebbecke, G. E. Meyer, K. Von Bargen, and D. A. Mortensen, "Shape features for identifying young weeds using image analysis," *Trans. ASAE (American Soc. Agric. Eng.*, vol. 38, no. 1, pp. 271–281, 1995.

[12] M. Guijarro, G. Pajares, I. Riomoros, P. J. Herrera, X. P. Burgos-Artizzu, and A. Ribeiro, "Automatic segmentation of relevant textures in agricultural images," *Comput. Electron. Agric.*, vol. 75, no. 1, pp. 75–83, 2011.

[13] P. Srestasathiern and P. Rakwatin, "Oil palm tree detection with high resolution multi-spectral satellite imagery," *Remote Sens.*, vol. 6, no. 10, pp. 9749–9774, 2014.

[14] W. Yang, S. Wang, X. Zhao, J. Zhang, and J. Feng, "Greenness identification based on HSV decision tree," *Inf. Process. Agric.*, vol. 2, no. 3–4, pp. 149–160, 2015.

[15] G. E. Meyer and J. C. Neto, "Verification of color vegetation indices for automated crop imaging applications," *Comput. Electron. Agric.*, vol. 63, no. 2, pp. 282–293, 2008.

[16] J. Camargo Neto, "A combined statistical - soft computing approach for classification and mapping weed species in minimum tillage systems," *ETD Collect. Univ. Nebraska - Lincoln*, p. 340, 2004.

[17] C. J. Tucker, "Red and photographic infrared linear combinations for monitoring vegetation," *Remote Sens. Environ.*, vol. 8, no. 2, pp. 127–150, 1979.

[18] S. Perez, A. J., Lopez, F., Benlloch, J. V., & Christensen, "Colour and shape analysis techniques for weed detection in cereal fields," *Comput. Electron. Agric.*, vol. 25, no. 3, pp. 197–212, 2000.

[19] M. J. Falkowski, P. E. Gessler, P. Morgan, A. T. Hudak, and A. M. S. Smith, "Characterizing and mapping forest fire fuels using ASTER imagery and gradient modeling," *For. Ecol. Manage.*, vol. 217, no. 2–3, pp. 129–146, 2005.

[20] T. Motohka, K. N. Nasahara, H. Oguma, and S. Tsuchida, "Applicability of Green-Red Vegetation Index for remote sensing of vegetation phenology," *Remote Sens.*, vol. 2, no. 10, pp. 2369–2387, 2010.

[21] T. Waser, L. T., Küchler, M., Jütte, K., & Stampfer, "Evaluating the potential of WorldView-2 data to classify tree species and different levels of ash mortality," *Remote Sens.*, vol. 6, no. 5, pp. 4515–4545, 2014.

[22] A. A. Gitelson, Y. J. Kaufman, and M. N. Merzlyak, "Use of a green channel in remote sensing of global vegetation from EOS-MODIS," *Remote Sens. Environ.*, vol. 58, no. 3, pp. 289–298, 1996.

[23] E. R. Hunt *et al.*, "NIR-Green-Blue high-resolution digital images for assessment of winter cover crop biomass," *GIScience Remote Sens.*, vol. 48, no. 1, pp. 86–98, 2011.

[24] H. Nouri, S. Beecham, S. Anderson, and P. Nagler, “High spatial resolution WorldView-2 imagery for mapping NDVI and its relationship to temporal urban landscape evapotranspiration factors,” *Remote Sens.*, vol. 6, no. 1, pp. 580–602, 2013.

[25] B. Gwata, “Developing high resolution clutter for wireless network propagation using WorldView-2 imagery,” *SPIE Defense, Secur. Sens.*, vol. 8390, p. 83902Q--83902Q, 2012.

[26] R. P. Sripada, “Determining in-season nitrogen requirements for corn using aerial color-infrared photography,” no. v, 2005.

[27] A. K. Verma, P. K. Garg, K. S. H. Prasad, and V. K. Dadhwal, “Classification of LISS IV imagery using decision tree methods,” *Int. Arch. Photogramm. Remote Sens. Spat. Inf. Sci. - ISPRS Arch.*, vol. 41, no. July, pp. 1061–1066, 2016.

[28] J. W. Rouse, R. H. Hass, J. A. Schell, and D. W. Deering, “Monitoring vegetation systems in the great plains with ERTS,” *Third Earth Resour. Technol. Satell. Symp.*, vol. 1, pp. 309–317, 1973.

[29] J. Xue and B. Su, “Significant remote sensing vegetation indices: A review of developments and applications,” *J. Sensors*, vol. 2017, 2017.

[30] S. Eckert, “Improved forest biomass and carbon estimations using texture measures from WorldView-2 satellite data,” *Remote Sens.*, vol. 4, no. 4, pp. 810–829, 2012.

[31] V. Marshall, M. Lewis, and B. Ostendorf, “Do additional bands (coastal, nir-2, red-edge and yellow) in WorldView-2 multispectral imagery improve discrimination of an invasive tussock, buffel grass,” *ISPRS - Int. Arch. Photogramm. Remote Sens. Spat. Inf. Sci.*, vol. XXXIX-B8, no. September, pp. 277–281, 2012.

[32] T. Santos and S. Freire, “Testing the contribution of WorldView-2 improved spectral resolution for extracting vegetation cover in urban environments,” *Can. J. Remote Sens.*, vol. 41, no. 6, pp. 505–514, 2015.

[33] O. Niemann, D. Adams, and G. Hay, “Automated tree crown identification using digital orthophoto mosaics,” *Int. Forum Autom. Interpret. High Spat. Resolut. Digit. Imag. For.*, pp. 127–139, 1999.

[34] M. Wulder, K. O. Niemann, and D. G. Goodenough, “Local maximum filtering for the extraction of tree locations and basal area from high spatial resolution imagery,” *Remote Sens. Environ.*, vol. 73, no. 1, pp. 103–114, 2000.

[35] S. Šumbera and V. Židek, “Digital classification of tree species and spatial structure of forest stands from remotely sensed data,” vol. 1990, pp. 439–446, 2003.

[36] I. Smits, G. Prieditis, S. Dagis, and D. Dubrovskis, “Individual tree identification using combined lidar data and optical imagery,” *Res. Rural Dev. 2012, Vol 2*, vol. 1, pp. 7–13, 2012.

[37] N. Khalid, J. R. A. Hamid, and Z. A. Latif, “Accuracy assessment of tree crown detection using local maxima and multi-resolution segmentation,” *IOP Conf. Ser. Earth Environ. Sci.*, vol. 18, no. 1, p. 012023, 2014.

[38] V. J. D. Tsai, “A comparative study on shadow compensation of color aerial images in invariant color models,” *IEEE Trans. Geosci. Remote Sens.*, vol. 44, no. 6, pp. 1661–1671, 2006.

[39] A. Khekade and K. Bhoyar, “Shadow detection based on RGB and YIQ color models in color aerial images,” *2015 1st Int. Conf. Futur. Trends Comput. Anal. Knowl. Manag. ABLAZE 2015*, no. Ablaze, pp. 144–147, 2015.

[40] H. D. Sevim, “Shadow detection on multispectral images,” Middle East Technical University, 2015.

[41] H. Dağlayan Sevim, Y. Yardımcı Çetin, and D. Özışık Başkurt, “A novel method to detect shadows on multispectral images,” no. October 2016, p. 100040A, 2016.

[42] C. Mei and S. Durrieu, “Tree crown delineation from digital elevation models and high resolution imagery,” *Proc. Int. Arch. Photogramm. Remote Sens. Spat. Inf. Sci.*, pp. 218–223, 2004.

[43] A. O. Ok, “Automated detection of buildings from single VHR multispectral images using shadow information and graph cuts,” *ISPRS J. Photogramm. Remote Sens.*, vol. 86, pp. 21–40, 2013.

[44] N. Otsu, “A threshold selection method from gray-level histograms,” *IEEE Trans. Syst. Man. Cybern.*, vol. 9, no. 1, pp. 62–66, 1979.

[45] M. F. Gomes and P. Maillard, “Identification of urban tree crown in a tropical environment using WorldView-2 data: problems and perspectives,” *SPIE Remote Sensing*, vol. 8893, no. 31. p. 88930C, 2013.

[46] M. Mahour, V. Tolpekin, and A. Stein, “Tree detection in orchards from VHR satellite images using scale-space theory,” vol. 10004, pp. 1–17, 2016.

APPENDICIES

APPENDIX A

TREE DETECTION RESULTS

In this section, four more different images which are cropped from WorldView-2 and WorldView-3 multispectral imagery are represented for further visual inspection. Since ground truth data does not exist for these scenes, only detected treetops and removed treetops marked. In Figure 39-41, detected treetops are shown as red plus sign and the removed local peaks by shadow based validation are marked as blue circles.

Figure 39: Results of sample WorldView-2 scene

Figure 40: Results of sample WorldView-3 scene

Figure 41: Results of sample WorldView-3 scene

TEZ FOTOKOPİ İZİN FORMU

ENSTİTÜ

Fen Bilimleri Enstitüsü ☐

Sosyal Bilimler Enstitüsü ☐

Uygulamalı Matematik Enstitüsü ☐

Enformatik Enstitüsü ☒

Deniz Bilimleri Enstitüsü ☐

YAZARIN

Soyadı : ONAĞ

Adı : Mehmet Mert

Bölümü : Bilişim Sistemleri

TEZİN ADI (İngilizce): Tree Crown Detection Using Multispectral Satellite Imagery

TEZİN TÜRÜ: Yüksek Lisans ☒ Doktora ☐

1. Tezimin tamamı dünya çapında erişime açılsın ve kaynak gösterilmek şartıyla tezimin bir kısmı veya tamamının fotokopisi alınsın. ☐
2. Tezimin tamamı yalnızca Orta Doğu Teknik Üniversitesi kullancılarının erişimine açılsın. (Bu seçenekle tezinizin fotokopisi ya da elektronik kopyası Kütüphane aracılığı ile ODTÜ dışına dağıtılmayacaktır.) ☒
3. Tezim bir (1) yıl süreyle erişime kapalı olsun. (Bu seçenekle tezinizin fotokopisi ya da elektronik kopyası Kütüphane aracılığı ile ODTÜ dışına dağıtılmayacaktır.) ☐

Yazarın imzası ..... Tarih .....